Geochemistry, Geophysics, Geosystems

RESEARCH ARTICLE
10.1029/2018GC007832

Key Points:
- This is a stratigraphically classified tephra database of glass compositions with correlations of marine and terrestrial tephra layers
- We provide new insights into the lifetime of the major volcanic centers in Guatemala and El Salvador and their number of major eruptions
- We identify five pulses of enhanced volcanic activity during the Quaternary, the Pliocene, the Late, Middle Miocene, and Early

Supporting Information:
- Supporting Information S1
- Table S1

Correspondence to:
J. C. Schindlbeck,
julie.schindlbeck@geow.uni-heidelberg.de

Citation:
Schindlbeck, J. C., Kutterolf, S., Freundt, A., Eisele, S., Wang, K.-L., & Frische, M. (2018). Miocene to Holocene marine tephrostratigraphy offshore northern Central America and southern Mexico: Pulsed activity of known volcanic complexes. *Geochemistry, Geophysics, Geosystems*, *19*, 4143–4173. https://doi.org/10.1029/2018GC007832

Received 16 JUL 2018
Accepted 26 SEP 2018
Accepted article online 28 SEP 2018
Published online 5 NOV 2018

Miocene to Holocene Marine Tephrostratigraphy Offshore Northern Central America and Southern Mexico: Pulsed Activity of Known Volcanic Complexes

J. C. Schindlbeck[1], S. Kutterolf[2], A. Freundt[2], S. Eisele[3], K.-L. Wang[4,5], and M. Frische[2]

[1]Institute of Earth Sciences, Heidelberg University, Heidelberg, Germany, [2]GEOMAR Helmholtz Centre for Ocean Research Kiel, Kiel, Germany, [3]Asian School of the Environment, Nanyang Technological University, Singapore, [4]Institute of Earth Sciences, Academia Sinica, Taipei, Taiwan, [5]Department of Geosciences, National Taiwan University, Taipei, Taiwan

Abstract We studied the tephra inventory of 14 deep sea drill sites of three Deep Sea Drilling Project and Ocean Drilling Program legs drilled offshore Guatemala and El Salvador (Legs 67, 84, and 138) and one leg offshore Mexico (Leg 66). Marine tephra layers reach back from the Miocene to the Holocene. We identified 223 primary ash beds and correlated these between the drill sites, with regions along the volcanic arcs, and to specific eruptions known from land. In total, 24 correlations were established between marine tephra layers and to well-known Quaternary eruptions from El Salvador and Guatemala. Additional 25 tephra layers were correlated between marine sites. Another 108 single ash layers have been assigned to source areas on land resulting in a total of 157 single eruptive events. Tephra layer correlations to independently dated terrestrial deposits provide new time markers and help to improve or confirm age models of the respective drill sites. Applying the respective sedimentation rates derived from the age models, we calculated ages for all marine ash beds. Hence, we also obtained new age estimates for eight known but so far undated large terrestrial eruptions. Furthermore, this enables us to study the temporal evolution of explosive eruptions along the arc, and we discovered five pulses of increased activity: (1) a pulse during the Quaternary, (2) a Pliocene pulse between 6 and 3 Ma, (3) a Late Miocene pulse between 10 and 7 Ma, (4) a Middle Miocene pulse between 17 and 11 Ma, and (5) an Early Miocene pulse (ca. >21 Ma).

1. Introduction

Understanding the long-term evolution of volcanic systems is one important way of assessing future volcanic hazards (e.g., Freundt et al., 2006; Kutterolf et al., 2013). This is especially important for regions along volcanic arcs that are highly populated and therefore particularly vulnerable in case of a natural catastrophe. Highly explosive volcanism is an essential part of the arc volcanism particularly in ocean-continent subduction zones and is assumed to be representative for the entire arc volcanism in these regions (e.g., Deligne et al., 2010; Mason et al., 2004; Pyle, 1995). Widely distributed ash, as one major eruptive product, is best preserved in mostly nonerosive marine and lacustrine environments, which thus provide the most complete record of such highly explosive volcanic activity over long time scales (Carey, 2000; Carey & Sigurdsson, 2000; Keller et al., 1978; Kutterolf, Freundt, Peréz, et al., 2008; Ledbetter, 1985; Schindlbeck, Kutterolf, Freundt, Alvarado, et al., 2016; Schindlbeck, Kutterolf, Freundt, Andrews, et al., 2016; Schindlbeck, Kutterolf, Freundt, Straub, et al., 2016). Wide areal distribution across sedimentary facies boundaries, near-instantaneous emplacement, unambiguous chemical compositions, and the presence of minerals suitable for radio-isotopic dating make the deposits of volcanic eruptions to excellent stratigraphic marker beds in terrestrial and marine sediments. Furthermore, they provide constraints on the temporal evolution of both the volcanic source region and the ash-containing sediment facies (e.g., Kutterolf, Freundt, Peréz, et al., 2008; Kutterolf, Freundt, & Peréz, 2008; Kutterolf, Freundt, Schacht, et al., 2008; Kutterolf, Liebetrau, et al., 2008; Kutterolf et al. 2016; Ponomareva et al., 2013, 2015, 2017; Schindlbeck, Kutterolf, Freundt, Alvarado, et al., 2016; Schindlbeck, Kutterolf, Freundt, Andrews, et al., 2016; Schindlbeck, Kutterolf, Freundt, Straub, et al., 2016).

In this contribution we focus on tephrostratigraphic correlations between Deep Sea Drilling Project (DSDP) and Ocean Drilling Program (ODP) sites and the correlation of marine tephras to volcanic complexes and eruptions from Central America. The investigated DSDP/ODP sites are located in the Pacific Ocean offshore the southernmost end of the Trans-Mexican Volcanic Belt (TMVB; Leg 66 drilled in 1979; Watkins et al., 1981) and offshore the northern Central American Volcanic Arc (CAVA) in Guatemala and El Salvador

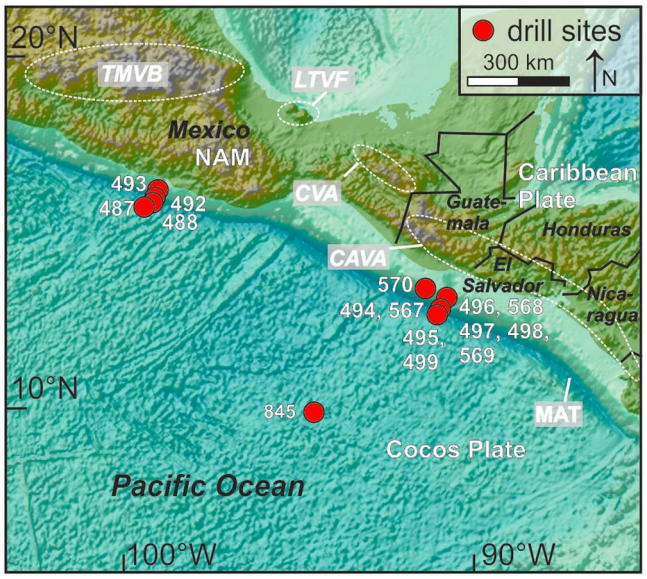

Figure 1. Overview map of Central America with the major volcanic regions in southern Mexico, Guatemala, and El Salvador. Map created using GeoMapApp (http://www.geomapapp.org; global multiresolution topography; Ryan et al., 2009). TMVB = Trans Mexican Volcanic Belt; LTVF = Los Tuxtlas Volcanic Field; CVA = Chiapanecan Volcanic Arc; CAVA = Central American Volcanic Arc; MAT = Middle American Trench; NAM = North American Plate. Red circles indicate drill site positions of deep-sea drilling programs.

(Figures 1 and 2; Leg 67 drilled in 1979, Leg 84 drilled in 1982, and Leg 138 drilled in 1991; Aubouin et al., 1982; Mayer et al., 1992; von Huene et al., 1985). Both arcs are known for numerous Quaternary Plinian and ignimbrite producing eruptions that generated widely dispersed pumice and ash deposits.

The overarching goal of this contribution is to establish a most complete chronotephrostratigraphy for highly explosive eruptions in this region that reaches back to the Early Miocene offshore Guatemala and El Salvador and back to the Late Miocene offshore Mexico. The results contribute to the discussion how the Late Cenozoic explosive volcanism in northern Central America evolved through time and provide new insights into the longevity of known Pleistocene volcanic centers.

2. Geological Background and Tephrostratigraphy

The volcanic arcs from Mexico, Guatemala, and El Salvador are located above the subduction zones of the Cocos Plate and Rivera Microplate that subduct beneath the Caribbean Plate (convergence rate of 70–90 mm/a; Barckhausen et al., 2001; DeMets, 2001) and the North American Plate (Figures 1 and 2). The CAVA extends continuously from the Mexican-Guatemalan border over ~1,100 km to central Costa Rica parallel to the Middle American Trench (MAT; Figure 1). The TMVB in Mexico is not parallel to the MAT but extends continuously over 1,000 km from West to East away from the trench (Figure 1). Volcanism in Mexico, south of the TMVB, is discontinuous and limited to isolated fields that are also not parallel to the trench (Mora et al., 2007); these include the Chiapanecan Volcanic Arc (CVA) and the Los Tuxtlas Volcanic Field (LTVF; Ferrari et al., 2012; Figure 1). Slightly oblique subduction at both, the Northern Central American (El Salvador and Guatemala) as well as the Mexican arc systems, occurs beneath a thick continental crust (40 km). Both subduction systems are erosional convergent margins resuming in high sedimentation rates due to rapid shortening and deepening depositional systems in the forearc (Clift & Vannucchi, 2004).

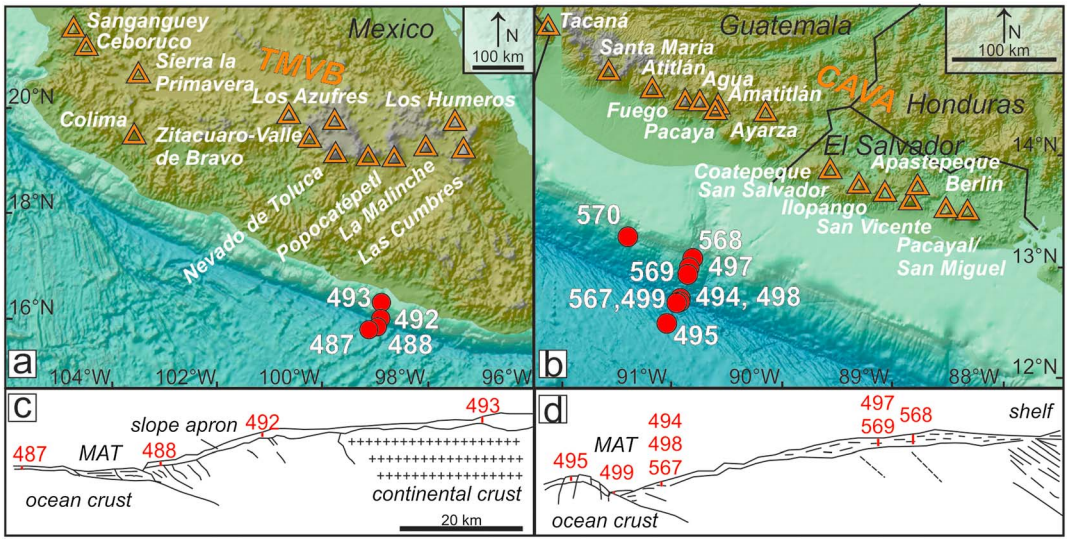

Figure 2. Maps of (a) the TMVB in Mexico and (b) the CAVA in Guatemala and El Salvador. Orange triangles mark positions of major Quaternary volcanoes along the arcs. Red circles indicate drill site locations of deep-sea drilling programs. (c and d) Schematic profiles perpendicular to the subduction zone showing sites located on the continental slope and incoming plate offshore Mexico (Sites 487, 488, 492, and 493) and offshore Guatemala (Sites 494–499 and 568–570). MAT = Middle American Trench; TMVB = Trans Mexican Volcanic Belt; CAVA = Central American Volcanic Arc.

2.1. CAVA

Along the CAVA, the slightly oblique subduction causes tectonic segmentation of the arc (DeMets, 2001; Funk et al., 2009), and subduction conditions such as state of hydration of the Cocos Plate and composition of its sediment cover, slap dip angle, and upper-plate crustal thickness and composition vary significantly along the subduction zone (Abers et al., 2003; Carr, 1984; Hoernle et al., 2002; Plank et al., 2002; Syracuse & Abers, 2006). This causes systematic regional variations in geochemical compositions of Quaternary volcanic rocks along the arc and between arc segments, which have been extensively studied (e.g., Carr, 1984; Carr et al., 1990, 2003; 2007; Feigenson & Carr, 1986; Feigenson et al., 2004; Freundt et al., 2014; Hoernle et al., 2008; Patino et al., 1997, 2000). Principal variations of major element are Na_2O decreases from Guatemala to Nicaragua and subsequent increase in Central Costa Rica (Carr, 1984; Carr et al., 2007), while FeO varies inversely with Na_2O, which Plank and Langmuir (1988) explain with changes of crustal thickness (high Na_2O and low FeO where the crust is thicker). In Central and NW Costa Rica, the volcanic rocks of the last 6 Myr carry the ocean island signature of the subducted Cocos Ridge (e.g., Carr et al., 2007; Gazel et al., 2009; Schindlbeck, Kutterolf, Freundt, Straub, et al., 2016). The Ba/La, Ba/Th, and U/Th ratios are the highest in Nicaragua and decrease toward Guatemala as well as to Costa Rica, which can be attributed to a higher slab sediment component and high fluid flow (Cameron et al., 2002; Carr et al., 1990). The La/Yb ratio instead shows an inverse variation to Ba/La (Carr et al., 2007) and is a proxy for the degree of melting (Cameron et al., 2002). High Rb/Hf and Th/Nb ratios in Guatemala and northern El Salvador possibly indicate a crustal melt signature (Hannah et al., 2002; Heydolph et al., 2012; Walker et al., 2007).

In the northern part of the arc, volcanic activity can be dated back to the Eocene (Donnelly et al., 1990). During Quaternary and Pliocene to Miocene times, large caldera systems in El Salvador/Honduras and Guatemala produced large-magnitude eruptions of highly evolved, silicic magmas (e.g., Jordan, Sigurdsson, Carey, Rogers, et al., 2007; Jordan, Sigurdsson, Carey, Lundin, et al., 2007; Reynolds, 1980, 1987; Rose et al., 1999; Weyl, 1980), and some of these large eruptions contributed also to the marine tephra record offshore the southern CAVA (Jordan et al., 2006; Kutterolf, Freundt, Peréz, et al., 2008; Schindlbeck, Kutterolf, Freundt, Alvarado, et al., 2016; Schindlbeck, Kutterolf, Freundt, Straub, et al., 2016). The stratigraphy of several highly explosive eruptions from, for example, Ilopango, Coatepeque, Ayarza, Amatitlán, and Atitlán calderas is quite well known for late Pleistocene times (e.g., Koch & McLean, 1975; Kwasnitschka, 2009; Rose et al., 1987, 1999). But less is known about older eruptions from ancestor volcanic systems. The major tephra deposits for the modern calderas from El Salvador and Guatemala are summarized in Figure 3 and Table 1.

2.2. Mexican Volcanic Arcs

Two major volcanic provinces exist in Mexico during the Cenozoic; the Sierra Madre Occidental (Eocene–Middle Miocene) and the TMVB (Miocene–Recent; e.g., Verma & Carrasco-Núñez, 2003). The arc of the Sierra Madre Occidental strikes north to northwest and lies north of the east-west trending TMVB (outside the northern bounds of Figures 1 and 2a). The relationship and temporal transition of volcanic activity from the Sierra Madre Occidental to the TMVB are still under discussion but accompanied by a shift in the predominant volcanic products from evolved ignimbrites and rhyolites to andesitic and basaltic lavas (e.g., Ferrari et al., 1999; Morán-Zenteno et al., 1999; Verma & Carrasco-Núñez, 2003). Lenhardt et al. (2010, 2011) postulate an initial phase of the TMVB retained in the Tepoztlán Formation that reaches back to the Early Miocene.

Volcanism in the TMVB is dominated by calc-alkaline Neogene to Quaternary cones, maars, domes, and stratovolcanoes, but several areas with alkaline volcanism exist. Several workers proposed genetic models for the TMVB that vary from the classical subduction model, for example, a mantle plume (e.g., Márquez et al., 1999; Moore et al., 1994) or continental rifting (Sheth et al., 2000; Verma, 2002), to explain the geochemical variations (a review on the TMVB evolution is provided by Ferrari et al., 2012). Detailed tephrostratigraphic studies have been conducted mainly on Holocene to Late Pleistocene deposits (e.g., Newton & Metcalfe, 1999; Ortega-Guerrero & Newton, 1998), whereas studies of Early Pleistocene and Neogene tephra sequences are rare. Several volcanic complexes have produced large eruptions during the Holocene and the Late Pleistocene. A summary of these eruptions is presented in Table 2.

South of the TMVB, the volcanism in the Mexican CVA (Figure 1) is dominated by dome volcanism and associated phreatomagmatic explosive volcanism (Mora et al., 2007). However, El Chichón Volcano, the youngest edifice of the CVA (Damon & Montesinos, 1978), is also known for historical and Holocene highly explosive

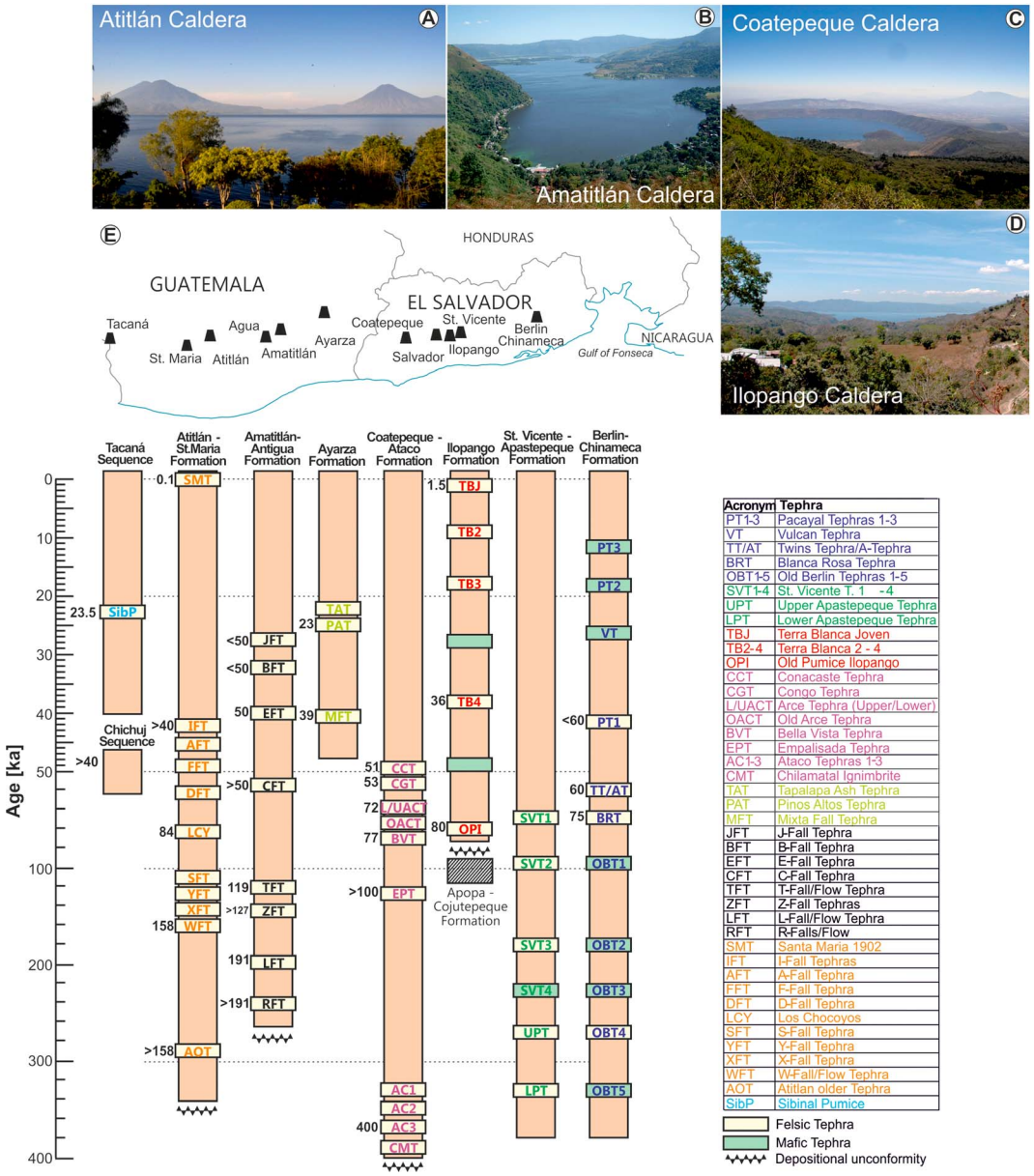

Figure 3. (a–d) Pictures of large caldera systems in northern Central America. (e) Simplified composite stratigraphic successions of known Late Pleistocene/Holocene tephras from highly explosive eruptions in northern Central America (modified from Kutterolf, Liebetrau, et al., 2008; Kutterolf et al., 2016) along the northern part of the Central American Volcanic Arc; tephra acronyms of respective eruptions are given in the table to the right. Each color represents one formation. Yellow bars mark silicic tephras, and green bars mafic widespread tephras. Major unconformities in the successions are shown by black zigzag bands. Individual numbers next to tephra layers give known eruption ages (Kutterolf, Freundt, & Peréz, 2008). Tephras without numbers are estimated on the basis of field observations (e.g., thickness of soils and sediments). See Table 1 for comparison.

Plinian eruptions (Espindola et al., 2000; Macías et al., 2003). Little is known about earlier eruptions, although rocks of the volcano flanks were dated to ~200,000–280,000 years BP by K-Ar techniques (Damon & Montesinos, 1978; Duffield et al., 1984).

The LTVF is located on the Gulf of Mexico coastal plain, ~200 km southeast of the TMVB, and consist mainly of scoria cones and maars and four major volcanic edifices (Sieron et al., 2014). Lavas of the LTVF have alkaline compositions, which is part of the debate, whether volcanism is related to subduction of the Cocos plate or to extensional tectonics (e.g., Nelson & Gonzales-Caver, 1992; Verma, 2006).

Geochemistry, Geophysics, Geosystems

10.1029/2018GC007832

Table 1
Summary Table of Major Explosive Eruptions of El Salvador and Guatemala

Volcanic source	Formation	Tephra deposit	Acronym	Age (ka)	Reference
El Salvador					
Berlin-Pacayal-Volcan Group	Berlin-Chinameca Formation	Old Berlin Tephras 1–5	OBT 1–5		CEL, 1995
		Blanca Rosa Tephra	BRT	75 ± 10; *D*	Kutterolf, Freundt, & Peréz, et al., 2008
		Twins/A-Tephra	TT/AT	60; *S*	Rohr, 2014
		Pacayal-1 Tephra	PT1	51–53 ka (stratigraphy)	
		Volcan Tephra	VT		
		Pacayal-2 Tephra	PT2		
		Pacayal-3 Tephra	PT3		
St-Vicente-Apastepeque	St-Vicente-Apastepeque Formation	Lower Apastepeque Tephra	LPT		
		Upper Apastepeque Tephra	UPT		
		St. Vicente Tephras 1–4	SVT1–4		
Ilopango Caldera	Ilopango Formation	Old Pumice Ilopango	OPI		Rose et al., 1999
		Terra Blanca 4	TB4	36; *S*	Mann et al., 2004
		Terra Blanca 3	TB3		Kutterolf, Freundt, Peréz, et al., 2008
		Terra Blanca 2	TB2		Kwasnitschka, 2009
		Terra Blanca Joven	TBJ	1.6; *D*	Dull et al., 2001
Coatepeque Caldera	Coatepeque-Ataco Formation	Bellavista Tephra	BVT	77 ± 2; *D*	Rose et al., 1999
		Lower and Upper Arce Tephra	L/UACT	72 ± 3; *D*	Kutterolf, Freundt, Peréz, et al., 2008
		Congo Tephra	CGT	53 ± 3	
		Conacaste Tephra	CCT	51	
Unknown; Coatepeque area	Coatepeque-Ataco Formation	Empalisada Tephra	EPT	350	CEL, 1992
Concepcíon de Ataco Caldera	Coatepeque-Ataco Formation	Chilamatal Ignimbrite	CMT	ca. 406; *S*	Partida et al., 1997
		Ataco Tephras 1–3	AC1–3	ca. 400; *S*	Siebert et al., 2010
					Kutterolf et al., 2016
Guatemala					
Ayarza Caldera	Ayarza Formation	Mixta Fall Tephra	MFT	39; *S*	Kutterolf, Freundt, Peréz, et al., 2008
		Piños Altos Tephra	PAT	23; *D*	Petersen & Rose, 1985
		Tapalapa flow	TAT	23; *D*	
Amatitlán Caldera-Antigua	Amatitlán-Antigua Formation	R-Fall Tephra	RFT	>500	Koch & McLean, 1975
		L-Fall Tephra	LFT	191 ± 11; *D*	Rose et al., 1999
		Z1-Z5- Fall Tephras	ZFT	>127; <182 (stratigraphy)	Kutterolf, Freundt, Peréz, et al., 2008
		T-Fall Tephra	TFT	119 ± 8; *D*	
		E-Fall Tephra	EFT	51; *S*	
Unknown	Associated with Amatitlán-Antigua Formation	C-Fall Tephra	CFT	>51; stratigraphy	Kutterolf et al., 2016
Atitlán Caldera	Atitlán-St. Maria Formation	W-Fall Tephra	WFT	158 ± 3; *D*	Rose et al., 1999
		H-Fall Tephra/Los Chocoyos	LCY	84 ± 5; oxygen isotope stratigraphy	Koch & McLean, 1975
					Drexler et al., 1980
		I2-I5-Fall Tephras	IFT	>40; stratigraphy	
Unknown	Associated Atitlán-St. Maria Formation	X-Fall Tephras	XFT	>119; <158; stratigraphy	Rose et al., 1999
		Y-Fall Tephras	YFT	>119; <158; stratigraphy	
		S-Fall Tephras	SFT	>119; <158; stratigraphy	
Tacaná Volcanic complex		Sibinal Pumice	SibP	23.5 ± 0.25	Arce et al., 2012

Note. Compare with Figure 3. *D* = radiometrically dated on land tephras; *S* = dated with sedimentation rates.

Table 2
Summary Table of Major Explosive Eruptions of Mexico

Volcanic source region	Eruptions/tephra deposits	Age/epoch	Reference
	Mexico		
Apan region	Matamoros Ignimbrite and pyroclastic flow deposits within the Peñon Andesites	ca. 13 Ma	García-Palomo et al., 2002
	Tecoloquillo Ignimbrite	42–31 ka	
Las Cumbres Volcanic complex including Pico de Orizaba Volcano	Several large eruptions	Holocene and Late Pleistocene	Robin & Cantagrel, 1982; Robin et al., 1983; Hoskuldsson & Robin, 1993; Carrasco-Nunez & Rose, 1995; Rossotti et al., 2006
Los Humeros Volcanic Center	Xáltipan Ignimbrite	0.46 Ma	Ferriz & Mahood, 1984
La Malinche Volcano	Three explosive eruptions	Within the last 40 ka	Siebe et al., 1995
Popocatépetl volcano	Numerous eruptions	Before 25–20 ka	Arana-Salinas et al., 2010;
	Large Plinian eruptions every 3–1 kyr	During the last 20 ka	Boudal & Robin, 1989; Siebe et al., 1995, 1996
Nevado de Toluca Volcano	Numerous Plinian eruptions	Between ca. 28 and 10 ka	Arce et al., 2003, 2005, 2013; Bloomfield & Valastro, 1974, 1977
Colima Volcano/Colima-Cantaro Chain	Several pyroclastic and lava eruptions	Tephrostratigraphy $<$10 ka	Robin et al., 1987
Sierra La Primavera complex	Tala Tuff	95 ka	Mahood, 1981; Mahood & Halliday, 1988
Cerborucu Volcano	Jala Pumice	ca. 1,000 years	Gardner & Tait, 2000
	Marquesado pyroclastic flow	ca. 1,000 years	

2.3. Previous Marine Studies

Several studies investigated the tephra inventory of DSDP/ODP/IODP (International Ocean Discovery Program) drill cores and sediment gravity cores along the MAT and in the Caribbean Sea (e.g., Bowles et al., 1973; Cadet, Pouclet, et al., 1982; Cadet, Thisse, et al., 1982; Clift et al., 2005; Jordan et al., 2006; Kutterolf et al., 2007; Kutterolf, Freundt, Peréz, et al., 2008; Ledbetter, 1985; Schindlbeck, Kutterolf, Freundt, Alvarado, et al., 2016; Schindlbeck, Kutterolf, Freundt, Andrews, et al., 2016; Schindlbeck, Kutterolf, Freundt, Straub, et al., 2016). Ash beds from the Pacific form a tephrostratigraphic framework of large CAVA and Galápagos eruptions back to the Miocene (Kutterolf et al., 2007; Kutterolf, Freundt, Peréz, et al., 2008; Schindlbeck et al., 2015; Schindlbeck, Kutterolf, Freundt, Alvarado, et al., 2016), whereas the ODP sites of the Caribbean Sea contain Neogene ash beds originated from source volcanoes at the Lesser Antilles and in Honduras and Nicaragua (Jordan, Sigurdsson, Carey, Lundin, et al., 2007; Carey & Sigurdsson, 2000; Sigurdsson et al., 2000). So far, however, the major and trace element geochemistry of the tephra inventory of the DSDP/ODP sites offshore North Central America and Mexico has not been studied in detail with respect to provenance and correlation to terrestrial deposits.

3. Methods

3.1. Sampling

The cores were sampled at the IODP Gulf Coast Repository at the Texas A&M University, College Station, TX, in 2013. We sampled four DSDP/ODP legs (Legs 66, 67, 84, and 138) with their corresponding three deep-sea drilling sites on the incoming Cocos Plate (Sites 487, 495, and 845), one in the MAT (Site 499), and 10 sites (Sites 488, 492, 493, 494, 497, 498, 567, 568, 569, and 570) on the continental slope offshore the northern CAVA and southern Mexico for the systematic investigation of ash beds intercalated in the deep marine sediments (Figure 1).

3.2. Methods and Analytical Techniques

Marine ash samples were disaggregated in an ultrasonic bath, if necessary, and subsequently wet-sieved into different grain size fractions (63–125, 125–250, $>$250 μm and if necessary 32–63 μm). The 63–125-μm fraction was further used for compositional analysis of glass shards with the electron microprobe (EMP) and Laser Ablation-Inductively Coupled Plasma-Mass Spectrometry (LA-ICP-MS). All major and trace element data are given in supporting information Tables S1–S6; for standard analyses, see supplement of Schindlbeck, Kutterolf, Freundt, Alvarado et al. (2016) and Kutterolf et al. (2014). Sampling and analytical methods

concord with the methods applied in Kutterolf, Freundt, Peréz, et al. (2008), Kutterolf et al. (2014, 2016, 2018), Schindlbeck et al. (2015), Schindlbeck, Kutterolf, Freundt, Alvarado, et al. (2016), and Schindlbeck et al. (2018).

3.2.1. EMP

Glass shard analyses (~3,500 in total) for major and minor elements were conducted on epoxy embedded samples using a JEOL JXA 8200 wavelength dispersive EMP at GEOMAR, Kiel adopting the methods from Kutterolf et al. (2011). Accuracy was monitored by standard measurements on Lipari obsidian (rhyolite; Hunt & Hill, 2001) and Smithsonian basaltic standard 'VGA'. Sixty individual glass shard measurements are bracketed by two standard measurements per standard. Standard deviations of measured elements are $<$0.5% for major and $<$10% for minor elements (with the exception of P_2O_5 and MnO_2 in samples $>$65 wt% SiO_2). All analyses are normalized to 100% to eliminate the effects of variable postdepositional hydration and minor deviations in focusing the electron beam; analyses with total oxides less than 90 wt% were excluded from the data set to avoid the effects of alteration. Finally, ~3,000 microprobe analyses passed the quality check which also excluded accidental shots on microcrystals. The remaining analyses for each sample were averaged (unless there was clear evidence for systematic compositional zonation) in order to characterize the elemental compositions of each individual tephra.

3.2.2. LA-ICP-MS

Trace and selected main element concentrations of ~750 glass shards were measured by LA-ICP-MS mainly at two laboratories in Taipei, Taiwan (between 2013 and 2016) as well as at GEOMAR Helmholtz Center for Ocean Research Kiel (Germany) in April 2011.

The LA-ICP-MS analyses at GEOMAR were made using a double-focusing, magnetic sector mass spectrometer (Nu-Instruments, AttoM), which is coupled to a 193-nm Excimer laser ablation system (Coherent, GeoLasPro). Ablation was performed in a pure Helium atmosphere; additionally, Argon carrier gas was mixed to the sample aerosol prior to the plasma torch. Spot analyses were done by 100-s ablation at a laser repetition rate of 3 Hz using a spot diameter of 16 μm and a fluence of 8 J/cm^2. Fifty-second gas background was collected prior to each ablation. Gas flows, torch position, and ion-optics focusing were optimized in order to provide a maximum in ion transparency, low oxide production rates (ThO/Th $\leq$ 0.3%), and fast sample washout. The standard NIST SRM610 glass (Wise & Watters, 2012) was used for mass calibration. Data were reduced by applying the linear regression slope method (Fietzke et al., 2008). Silicon was used for internal standardization utilizing data from EMP analyses.

The detailed machine setups, procedures, and methods of the laboratories at the National Taiwan University are described in Schindlbeck et al. (2015) and are complemented here by the description of the analytical procedures done during the measurements at the Academia Sinica (Schindlbeck, Kutterolf, Freundt, Andrews, et al., 2016). The setup at the Academia Sinica in Taipei, Taiwan, comprises a laser beam (193-nm excimer laser) set to a spot size of 16 to 30 μm using 5–10-J/cm^2 energy density at 4–10-Hz repetition rate which was coupled to high-resolution ICPMS instruments. Following 45 s of blank acquisition, typical ablation times were around 75 s. Data reduction was performed using version 4.0 of *real-time on-line* GLITTER© software (van Achterberg et al., 2001) immediately following each ablation analysis. Average silica and calcium concentrations, measured by EMP, were used as internal standards to normalize the trace element analyses. International standard glass (BCR-2G) was measured every five to eight samples to monitor accuracy and to correct for matrix effects and signal drift in the ICP-MS as well as for differences in the ablation efficiency between the sample and the reference material (Günther et al., 1999). Concentrations of NIST SRM 612, used for external calibration, were taken from Norman et al. (1996). The limit of detection for most trace elements is generally no greater than 100 ppb. For REEs (Rare Earth Elements), the limit of detection is generally around 10 ppb. The analytical precision is better than 10% for most trace elements. Repeated measurements of the same samples in different laboratories revealed good replication of the trace elements (Schindlbeck, Kutterolf, Freundt, Alvarado, et al., 2016).

3.3. Correlation Techniques

Geochemical fingerprinting of glass shards has been proved to be a reliable tool for tephra correlations (e.g., Kutterolf, Freundt, Peréz, et al., 2008; Kutterolf et al., 2016; Ponomareva et al., 2013, 2015; Lowe, 2011; Schindlbeck, Kutterolf, Freundt, Alvarado, et al., 2016). Correlations of ash beds to terrestrial deposits as well as between different marine sites are based on major and trace element concentrations and ratios (Kutterolf, Freundt, Peréz, et al., 2008; Kutterolf et al., 2016, 2018; Neugebauer et al., 2017; Schindlbeck et al., 2015;

Schindlbeck, Kutterolf, Freundt, Alvarado, et al., 2016; Schindlbeck et al., 2018; Wulf et al., 2004) as well as the relative stratigraphic positions and age constraints. For each marine ash bed, we carried out 15–20 EMP analyses, and the majority of marine ash beds were analyzed additionally for their trace element composition by LA-ICP-MS. For reference fields of onshore deposits, we used published major and trace element data (Kutterolf, Freundt, Peréz, et al., 2008; Kutterolf et al., 2016; Stoppa, 2015; Stoppa et al., 2018). In many cases, major element characteristics could not discriminate well between eruptions from single volcanoes, but then the trace element compositions of volcanic glass shards provided a unique "fingerprint" for each single eruption. Next to the comparison with terrestrial deposits, we also compared the investigated ash beds with data from previously studied marine drill cores (Schindlbeck, Kutterolf, Freundt, Alvarado, et al., 2016) and gravity cores (Kutterolf, Freundt, Peréz, et al., 2008) collected at the southern part of the CAVA.

3.4. Tephra Ages

Age data for the marine tephra layers initially came from the shipboard age-depth models derived from magnetostratigraphy and biostratigraphy from each site (Aubouin et al., 1982; Mayer et al., 1992; von Huene et al., 1985; Watkins et al., 1981). Marine tephra correlations to dated terrestrial tephra deposits (e.g., Koch & McLean, 1975; Kutterolf, Freundt, Peréz, et al., 2008; Rose et al., 1999; Stoppa et al., 2018) provide additional independent time markers and modified the existing age models (Figure S1). The ages of yet undated ash layers can be estimated from their relative position between known time markers (biostratigraphic time markers, paleomagnetic time markers, and correlations to independently dated terrestrial tephra deposits) by applying linear interpolation, which assumes constant sedimentation rates across such an interval. The relative position is determined from the thickness of (hemi)pelagic sediments alone, ignoring the thickness of other intercalated ash beds (Figure S1). We have used this method for all the marine tephra ages reported below (Tables 3, 4, and S1) that were not obtained by direct correlation with dated onland deposits.

Due to compaction and drilling disturbances, the tephra ages have higher uncertainties in deeper sections of each core (e.g., up to 14% of their age; c.f. Kutterolf et al., 2013). The ages of such horizons are therefore stated as approximate values in the discussion below.

Although we can justify the assumption of constant sedimentation rates across the relatively narrow interval between two known time markers at one site, the overall sedimentation rates vary quiet significantly along the arc and with time. We observe sedimentation rates of 5–273 m/Ma on the incoming plate and 30–1,540 m/Ma on the continental slope offshore Guatemala, up to 10,800 m/Ma near the trench axis at the mouth of the large San José submarine canyon, and 3–284 m/Ma offshore Mexico (Figure S1).

4. Results

4.1. Marine Tephra Inventory

In total, we sampled 295 ash beds and ash-rich horizons and identified 223 primary ash beds characterized by homogeneous to zoned glass compositions, in contrast to ash beds with mixed, genetically unrelated glass compositions, which we interpret as reworked deposits. In addition, we use the morphology and structure of the deposits to determine if they were reworked. The marine cores, especially from Legs 66 and 67 but also from Legs 84 and 138, are in parts heavily disturbed by rotary drilling (rotary core barrel) (Figure 4); advanced piston coring (APC) was not yet available at that time. We have sampled and analyzed tephra layers disturbed by drilling at multiple places in order to identify tephra that originally formed a single coherent layer. In these cases the stratigraphic position is determined by the uppermost occurrence of the tephra.

Although many ash beds are highly disturbed, also layers occur that are several centimeters to decimeter thick, which show normal grading and sharp contacts at the base and a diffuse transition into the background sediment at the top (Figure 4). Analyses of the glass shards dispersed in sediment above an ash layers typically reveals that they were reworked from that layer.

The DSDP Legs 66 and 67 took place in 1979 before advanced piston coring was available. Heavily disturbed cores and/or poor recovery thus disrupt the continuous stratigraphic record (Figure 4). Consequently, it is not surprising that tephra layers often cannot be correlated between several sites or holes although they might

Geochemistry, Geophysics, Geosystems

10.1029/2018GC007832

Table 3
Correlations of 24 Tephra Layers to Well-Known Eruptions from the Central American Volcanic Arc of the Last 1.8 Ma That Are Consecutively Numbered From C1 to C24

	Eruption (volcanic complex)	Marine tephra age (Ma)	Depth (mbsf)	Sample interval	K_2O (wt%)	SiO_2 (wt%)	MgO (wt%)	CaO (wt%)	La/Yb	Ba/La	Ba/Th	Rb/Hf	Zr/Nb
C1	TBJ (Ilopango)	<0.001	0.59	67-499-1R-CC, 0–20 cm	2.81	77.43	0.20	1.19	7.39	93.20	313.24	17.54	33.37
C2	LAT (Apoyo)	0.023	0.80	84-569-1H-1, 72–80 cm	3.01	75.48	0.34	1.68					
C3	TB4	0.002 (disturbed)	16.78	67-499A-3R-2, 78–89 cm	2.76	76.19	0.27	1.52	7.24	94.70	333.53	16.23	38.65
	(Ilopango)	0.025	14.70	67-496-2R-CC, 0–10 cm	2.70	77.52	0.19	1.16	7.82	90.29	361.99	19.31	25.44
		0.026	5.76	84-570*-2R-1, 96–103 cm	2.68	77.13	0.18	1.22	6.87	88.38	351.36	18.42	27.28
		0.035	20.54	67-496*-3R-3, 54–60 cm	2.73	77.12	0.19	1.17					
		0.036	21.27	67-496*-3R-3, 125–131 cm	2.72	77.14	0.20	1.20	6.76	88.59	320.90	17.79	26.95
		0.036	21.53	84-568-3H-6, 99–103 cm	2.72	77.39	0.17	1.13					
C4	MFT	0.025	14.70	67-496-2R-CC, 0–10 cm	4.21	77.26	0.07	0.40	9.45	40.94	104.32	49.59	6.43
	(Ayarza)	0.037	22.15	67-496-3R-4,–52–65 cm	4.09	76.93	0.06	0.42	8.15	41.89	104.22	43.66	7.54
		0.039	8.61	84-570*-2R-3, 81–86 cm	4.13	76.99	0.07	0.45	7.38	38.87	92.89	42.99	6.66
		0.048	40.21	67-496*-5R-2, 6–21 cm	4.01	77.24	0.06	0.41	5.32	55.97	109.52	52.93	4.88
		0.050	43.05	67-496-5R-4, 105–120 cm	4.12	77.23	0.06	0.40	6.24	53.85	110.03	45.09	4.77
		0.036	21.10	67-496*-3R-3, 110–124 cm	4.20	76.85	0.07	0.42					
C5	EFT	0.050	3.30	67-498-1H-3, 25–30 cm	3.64	77.34	0.14	0.90					
	(Amatitlán)	0.047	32.22	84-568-4H-CC, 5–10 cm	3.80	77.16	0.14	0.93					
		0.051	44.42	67-496*-5R-6, 92–97 cm	4.39	76.06	0.15	0.82	8.74	54.10	121.70	32.21	16.96
C6	CGT	0.053	38.75	84-568-5H-5, 38–45 cm	4.25	73.34	0.26	1.35	5.59	33.80	69.23	29.70	28.98
	(Coatepeque)	0.053	107.97	67-499*-13R-4, 53–57 cm	4.52	73.93	0.17	1.10	6.95	27.97	51.96	28.16	23.85
		0.058	12.68	67-497*-2R-5, 61–71 cm	4.42	73.46	0.20	1.33	7.34	38.12	72.07	27.71	26.64
C7	OPT	0.055	40.63	84-568-5H-6, 83–83 cm	1.25	57.59	2.21	7.65					
	(Berlin-Chinameca)	0.057	108.31	67-499*-13R-4, 87–92 cm	1.71	56.69	3.23	7.25	3.93	87.98	461.69	9.47	30.70
C8	IFT (Atitlán)	0.054	1.87	84-569*-2R-1, 67–68 cm	3.34	76.08	0.24	1.38					
C9	ACT (Coatepeque)	0.072	109.81	67-499*-13R-5, 99–112 cm	4.81	76.06	0.04	0.66	5.62	12.41	23.68	38.10	15.17
C10	LCY	Reworked	7.72	67-499-2R-5, 67–72 cm	3.80	77.83	0.11	0.86					
	(Atitlán)	Reworked	7.82	67-496-2R-1, 32–40 cm	4.07	77.80	0.08	0.65					
		Reworked	5.76	84-570*-2R-1, 96–103 cm	4.13	77.83	0.07	0.62					
		0.077	112.61	67-499*-13R-7, 108–117 cm	4.14	77.77	0.09	0.64	12.73	77.13	94.21	74.36	6.62
		0.084	5.02	67-494*-1R-4, 52–54 cm	4.23	77.97	0.09	0.65	12.84	78.27	97.80	66.79	6.68
		0.081	14.95	66-487-3R-3, 145–147 cm	3.92	78.15	0.08	0.63	13.61	67.83	88.76	70.62	8.29
		0.084	116.80	67-499-14R-2, 30–42 cm	4.19	77.89	0.09	0.63					
		0.084	51.11	67-496*-6R-4, 111–126 cm	4.05	77.80	0.12	0.90	15.79	50.55	74.32	57.95	10.34
		0.084	15.49	66-487-3R-4, 40–51 cm	3.84	78.36	0.09	0.65	13.75	75.88	96.84	68.71	6.60
		0.084	3.16	138-845B-1H-1, 6–9 cm	4.82	77.39	0.07	0.63					
		0.084	18.27	67-497*-3R-2, 127–137 cm	4.15	77.87	0.09	0.67	13.44	70.81	94.53	72.89	7.17
		0.084	41.52	84-568-5H-7, 15–17 cm	4.10	78.04	0.09	0.67	13.21	77.22	103.78	82.98	5.94
		0.084	10.32	84-570*-2R-4, 102–107 cm	3.80	77.49	0.11	0.79	11.69	83.18	107.30	81.13	6.08
C11	OPI (Ilopango)	0.084	5.02	67-494*-1R-4, 52–54 cm	2.75	77.16	0.20	1.29					
C12	OACT (Coatepeque)	0.092	45.98	84-568*-6R-3, 113–120 cm	4.00	75.00	0.17	1.13	5.70	86.71	185.41	22.49	37.20
C13	WFT	0.159	77.03	67-496*-9R-3, 113–114 cm	4.72	77.80	0.06	0.65	15.62	34.06	41.16	79.62	5.93
	(Atitlán)	0.159	37.90	67-497-5R-2, 120–130 cm	4.73	77.85	0.07	0.64	14.59	30.35	37.75	84.00	6.36
		0.159	8.73	84-567*-1R-7, 13–18 cm	5.04	77.06	0.05	0.68	13.33	32.49	56.17	39.87	8.59
		0.159	81.09	84-568-10H-1, 97–99 cm	4.87	77.10	0.12	0.68					
C14	LFT	0.191	32.19	66-487-5R-2, 119–123 cm	3.67	76.41	0.22	1.37	12.79	43.05	75.75	43.33	15.91
	(Amatitlán)	0.191	7.82	138-845-B-1H-5, 126–138 cm	4.09	76.99	0.13	0.79					
		0.191	54.44	84-570*-6R-6, 77–81 cm	4.05	76.79	0.13	0.86	12.69	46.69	103.98	40.07	11.91
C15	AOT	0.306	86.92	66-488*-11R-1, 42–45 cm	3.95	77.71	0.08	0.65	10.87	77.12	94.11	75.40	6.44
	(Atitlán)	0.268	53.29	66-487-7R-4, 29–35 cm	3.85	77.68	0.09	0.70	10.24	90.86	154.44	80.24	4.35

Table 3 *(continued)*

	Eruption (volcanic complex)	Marine tephra age (Ma)	Depth (mbsf)	Sample interval	K_2O (wt%)	SiO_2 (wt%)	MgO (wt%)	CaO (wt%)	La/Yb	Ba/La	Ba/Th	Rb/Hf	Zr/Nb
		0.306	63.59	66-487-8R-4, 107–112 cm	3.65	78.16	0.11	0.80	16.35	48.20	96.88	48.45	11.22
C16	AC3 (Ataco)	0.400	55.81	67-497*-7R-1, 131–145 cm	2.96	71.02	0.58	2.53					
C17	TolT (Malpaisillo)	0.420	60.18	84-570*-7R-3, 118–133 cm	2.99	72.21	0.43	1.87	3.67	110.09	603.99	14.80	38.47
		0.420	32.97	67-494-4R-CC, 0–20 cm	2.99	72.32	0.44	1.88	3.67	136.31	750.61	13.92	31.29
C18	LSabT (Malpaisillo)	0.451	58.32	67-497-7R-3, 82–87-2 cm	3.73	74.80	0.30	1.50	3.47	124.88	476.58	12.76	41.73
C19	Feliz (Ilopango)	0.660	22.94	84-569*-4R-2, 84–86 cm	3.08	77.39	0.17	1.22	7.64	94.71	299.08	23.36	25.55
C20	UPT (Apastepeque)	0.883	160.63	67-499-18R-6, 0–25 cm	3.15	76.65	0.23	1.35	10.05	101.18	311.62	23.76	22.63
C21	Salvamex (Ilopango)	1.025	23.36	67-495*-3R-3, 136–144 cm	3.11	77.98	0.19	1.29	10.48	97.11	231.88	25.16	27.15
C22	La Curva (Ilopango)	1.154	40.11	84-569*-6R-1, 11–14 cm	3.48	73.06	0.33	1.53	4.19	74.42	258.10	12.22	45.40
C23	LPT (Apastepeque)	1.549	197.19	67-499-22R-5, 48–52 cm	3.08	77.63	0.17	1.15	8.98	83.83	211.43	22.29	29.25
C24	LBBP (unknown)	1.843	113.83	67-494A-9R-1, 33–35 cm	2.53	75.25	0.33	2.04	4.80	167.35	754.16	16.64	52.44

be in close vicinity. By combining the different drill sites, we are confident to at least obtain a best-possible continuous record.

We sampled 26 ash horizons from four sites (Sites 487, 488, 492, and 493) of Leg 66 offshore Mexico and identified 22 primary tephra layers. In a previous study, Cadet, Pouclet, et al. (1982) sampled and analyzed 15 ash beds from Leg 66. We included their major element data for three ash beds from Sites 489, 490, and 491 and for four ash beds from sites 492 and 493 that we have not sampled. Geochemical analyses identified six tephra layers as primary tephra layers at incoming plate Site 487 intercalated with hemipelagic to pelagic mud, one at the lower slope site 488, nine at midslope Sites 490, 491, and 492 intercalated with hemipelagic mud, and seven at slope Sites 489 and 493 as primary tephra layers, whereas the others represent reworked or disturbed ash horizons. The marine ash beds of Leg 66 from offshore Mexico have rhyolitic glass compositions (Figure 5; >70 wt% SiO_2).

Eleven tephra layers were sampled from Site 845 of Leg 138, which is located ~600 km offshore of Guatemala. We identified five primary ash beds with ages obtained by shipboard age models scattering between Late Pleistocene, Early Pleistocene, and Late Miocene. All five are highly evolved rhyolites (>75 wt% SiO_2; Figure 5). Tephra layers are partly disturbed and embedded within diatom and radiolarian clay (0–136 mbsf) and nannofossil ooze (Mayer et al., 1992). Tephra thicknesses are hard to define, because the sediment is disturbed and bioturbated.

Two sites (Sites 495 and 499) were sampled from Leg 67 on the incoming plate offshore Guatemala and El Salvador. At Site 495, we took 22 samples and identified 19 primary, rhyolitic tephra layers (Figure 5) that occur between ~12–1-Ma old sediments (Watkins et al., 1981). Site 499 is located directly within the MAT, and we identified 13 primary tephra layers in Holocene to Middle Pleistocene sediments (Watkins et al., 1981). The majority of tephra layers are again highly evolved rhyolites, but we also identified one basaltic-andesitic tephra layer (~56 wt% SiO_2; Figure 5).

We took 224 samples from the eight slope sites from Legs 67 and 84 (Aubouin & von Huene, 1985; Mayer et al., 1982) and identified in total 164 primary ash beds embedded in Pleistocene to Early Miocene sediments. Tephra compositions are mainly rhyolitic and occasional basaltic-andesitic to dacitic (Figure 5). Thicknesses of tephra layers vary, and contacts are often disturbed or bioturbated, which nearly precludes exact thickness determination. The vast majority of the sampled tephra horizons are highly evolved, with SiO_2 concentrations ranging from ~70 to 78 wt% and total alkalis ranging from ~6 to 9.5 wt% (Figure 5). Only a small number of ash beds are less evolved, with SiO_2 concentrations below 60 wt% and total alkalis from 4 to 6 wt% (Figure 5). The shard morphology for these two geochemical groups is also generally consistent, while the glass shards of the highly evolved tephra layers are transparent to light brown, with rounded and elongated bubbles, and a fibrous texture (Figure 4). In comparison, glass shards from the less evolved group are light brownish, blocky, and less vesicular (Figure 4).

4.2. Correlation of Marine Tephras

In the following, we will present correlations of tephra layers to specific eruptions on land, between the sites along the arc and to the source volcanic complexes. We correlated 24 tephra layers to well-known eruptions from the CAVA of the last 1.8 Ma (Figures 6 and 7) that are consecutively numbered from *C1* to *C24* (Table 3). Additional 25 tephra layers were found in multiple marine drill or gravity cores along the arc and numbered from *S1* to *S25* (Figures 8 and 9; Table 4). All other ash beds solely appear once and are consecutively numbered for each site (#xx) and are associated to the source volcanic complexes (Figures 8 and 10). Provenance analyses that are shown below identified 21 volcanic events from Mexico, 36 from Guatemala, and 72 from El Salvador, as well as 14 from Nicaragua. For a subset of 14 tephra layers, the identification of the exact source region was not possible, because we had no trace element information and major elements alone are not sufficiently distinctive. All established correlations are given in Tables 3 and 4 and in supporting information S1. For better visualization, the

Geochemistry, Geophysics, Geosystems

10.1029/2018GC007832

Table 4
Correlations of 25 Tephra Layers That Were Found in Multiple Marine Drill or Gravity Cores Along the Arc That Are Consecutively Numbered From S1 to S25

	Correlation to source region along the arc	Age (Ma)	Depth (mbsf)	Sample interval	Correlated with tephra layer	K_2O (wt%)	SiO_2 (wt%)	MgO (wt%)	CaO (wt%)	La/Yb	Ba/La	Ba/Th	Rb/Hf	Zr/Nb
S1	Nicaragua	0.10	56.03	67-496*-7R-1, 103–112 cm	M66_223, 69–76 cm from Kutterolf, Freundt, Peréz et al. (2008)	1.27	55.96	3.37	7.66	3.95	99.41	543.95	11.03	33.90
S2	Nicaragua	0.16	76.94	67-496*-9R-3, 104–109 cm	*s3* (S-CAVA) from Schindlbeck, Kutterolf, Freundt, Alvarado, et al. (2016)	0.92	53.08	4.25	9.41	3.37	101.47	619.56	10.62	36.25
S3	Nicaragua	0.18	78.50	67-496*-9R-4, 117–143 cm	170-1039B-3H-3, 92–95 cm from Schindlbeck, Kutterolf, Freundt, Alvarado, et al. (2016)	1.31	56.19	3.33	7.78	3.09	104.58	658.26	10.02	34.07
S4	Nicaragua	0.21	80.32	67-496*-9R-6, 39–53 cm	170-1039B-3H-4, 120–123 cm from Schindlbeck, Kutterolf, Freundt, Alvarado, et al. (2016)	0.97	53.43	4.34	9.10	3.08	109.20	689.25	9.52	38.20
S5	Nicaragua	0.39	55.31	67-497*-7R-1, 81–91 cm	*s10* (S-CAVA) from Schindlbeck,	1.72	56.02	3.28	7.61	4.76	58.55	357.56	11.17	37.62
		0.43	93.99	67-496*-11R-1, 99–106 cm	Kutterolf, Freundt, Alvarado,	1.83	56.34	2.98	7.22	5.37	53.98	323.50	13.01	31.56
		0.42	14.64	84-569*-3R-3, 51–56 cm	et al. (2016)	1.35	57.48	3.16	7.24					
S6	Atitlán	0.51	38.23	67-494A-1R-1, 108–115 cm	M66-230, 397 cm from Kutterolf, Freundt, Peréz et al. (2008)	4.23	76.33	0.17	1.21	9.89	55.93	115.76	55.32	9.41
S7	Atitlán	0.54	39.70	67-494A-1R-2, 70–97 cm	M66-230, 412–416 cm from	3.91	77.61	0.15	0.90					
		0.57	41.40	67-494A-1R-3, 90–100 cm	Kutterolf, Freundt, Peréz et al. (2008)	3.99	77.56	0.14	0.83	12.73	48.72	109.76	52.58	8.79
S8	Ilopango	0.60	102.84	84-568-12H-5, 102–104 cm		2.46	63.81	1.61	4.12	4.60	53.58	219.07	13.62	37.85
		0.62	96.96	84-570*-11R-2, 96–99 cm		2.49	60.55	1.99	5.12	3.68	56.26	207.59	12.80	40.37
S9	Ayarza or Atitlán	1.01	34.95	84-569*-5R-4, 45–53 cm	*s21* (S-CAVA) from Schindlbeck, Kutterolf, Freundt, Alvarado, et al. (2016)	4.03	77.96	0.12	0.79	13.85	47.50	106.83	46.53	9.88
S10	Ilopango	1.40	141.57	84-568* 16R-4, 17–18 cm		3.30	76.17	0.25	1.42	5.12	99.71	369.67	15.95	31.66
		1.35	102.20	67-497*-12R-1, 20–23 cm		2.93	77.11	0.21	1.31	7.74	97.82	332.90	33.14	23.30
S11	Ilopango	1.62	152.71	84-568*-17R-4, 131–149 cm		2.99	75.35	0.23	1.39	7.62	95.41	342.33	18.58	34.26
		1.63	169.77	67-496*-19R-1, 77–82 cm		3.51	75.69	0.24	1.38	5.11	96.97	366.08	13.38	36.56
		1.67	38.05	67-495-5R-1, 5–12 cm		3.55	75.32	0.24	1.25					
		1.65	116.88	67-497*-13R-5, 93–108 cm		3.21	75.48	0.27	1.57	7.94	92.99	338.60	18.12	31.46
S12	Ilopango	2.20	191.50	84-570*-21R-1, 0–12 cm		3.68	77.35	0.11	0.95	9.58	82.27	219.74	48.48	17.09
		2.29	185.09	84-568-20H-7, 6–9 cm		3.76	77.47	0.19	1.10					
S13	Ilopango	2.21	50.44	67-495*-6R-3, 25–37 cm		3.74	73.61	0.29	1.25	4.31	64.71	205.02	11.40	49.10
		2.35	214.70	84-570*-23R-3, 100–105 cm		3.88	73.37	0.37	1.54	4.79	69.80	190.67	14.30	42.38
S14	Old Coyol Arc	2.26	51.52	67-495*-6R-3, 133–142 cm	170-1039B-11H-7, 41–44 cm from Schindlbeck, Kutterolf, Freundt, Alvarado, et al. (2016)	4.23	78.04	0.08	0.86	15.05	48.06	94.53	70.72	10.70
S15	Ilopango	2.89	228.97	67-496*-25R-4, 6–8 cm		3.98	68.97	0.67	2.39	4.30	81.69	200.49	13.86	42.63
		3.00	180.96	67-494A-16R-1, 96–104 cm		3.77	68.65	0.64	2.15	4.73	99.60	333.86	13.36	41.89
S16	Mexico	4.73	200.64	84-568*-22R-5, 39–40 cm		5.14	76.24	0.10	0.68	9.71	48.69	104.11	39.28	14.54
		4.84	189.38	66-493*-9R-2, 138–144 cm		5.32	75.72	0.13	0.66	8.24	33.15	66.96	39.83	11.63
		4.73	160.44	66-492*-18R-4, 21–95 cm		5.15	75.80	0.13	0.64	9.53	36.70	73.22	34.85	10.84
S17	Coatepeque/Ataco	6.32	134.12	67-495*-15R-1, 112–115 cm		4.86	73.91	0.29	1.16	8.81	36.41	89.88	29.47	29.49
		6.30	70.23	84-569*-9R-2, 38–47 cm		4.75	73.57	0.30	1.20	7.95	36.17	63.36	19.35	26.87
S18	Mexico	8.25	169.50	66-492*-19R-CC, 0–10 cm		4.68	76.06	0.14	0.65	9.18	30.49	56.89	34.40	14.71
		8.25	78.59	84-569*-10R-1, 69–79 cm		4.47	75.60	0.14	0.91	13.88	35.90	66.52	39.01	13.07
S19	Atitlán	13.82	267.15	84-567-8R-4, 5–14 cm		4.75	77.28	0.11	0.75	10.64	57.65	124.56	46.67	14.44
		13.95	249.15	84-568*-27R-4, 85–94 cm		5.15	77.32	0.11	0.71	12.36	69.76	125.88	43.89	15.66

Geochemistry, Geophysics, Geosystems

10.1029/2018GC007832

Table 4 *(continued)*

	Correlation to source region along the arc	Age (Ma)	Depth (mbsf)	Sample interval	Correlated with tephra layer	K_2O (wt%)	SiO_2 (wt%)	MgO (wt%)	CaO (wt%)	La/Yb	Ba/La	Ba/Th	Rb/Hf	Zr/Nb
S20	Ayarza or Ataco	14.28	267.52	84-568*-29R-3, 142–150 cm		4.80	75.58	0.18	0.79	7.79	31.90	66.14	33.18	16.39
		14.54	391.83	66-493*-30-R-4, 133–136 cm		4.60	75.96	0.16	0.71					
S21	Atitlán	14.32	269.86	84-568*-29R-5, 91–105 cm		4.84	77.32	0.11	0.62	7.83	65.92	104.68	66.79	6.61
		14.32	269.86	84-568*-29R-5, 91–105 cm		5.08	77.48	0.06	0.64	8.03	35.72	93.24	29.46	19.23
		14.43	88.15	84-569*-11R-1, 75–82 cm		5.19	77.46	0.06	0.61	11.89	48.50	85.50	40.37	11.45
	Coatepeque	14.32	269.86	84-568*-29R-5, 91–105 cm		3.87	77.61	0.09	0.82	14.14	10.88	15.52	67.77	6.45
S22	Amatitlán	15.77	352.33	84-568*-38R-2, 138–148 cm		4.87	77.53	0.08	0.55	10.74	51.26	92.60	49.37	9.67
		15.88	316.63	67-496*-34R-4, 63–71 cm		4.45	77.13	0.06	0.67	6.13	52.10	100.66	26.51	29.12
S23	Coatepeque/Ataco	15.34	192.18	67-494A-17R-2, 112–118 cm		5.45	74.33	0.21	0.78	8.86	42.55	73.07	25.75	23.01
		15.90	316.99	67-496*-34R-4, 99–108 cm		4.70	74.88	0.16	0.93	6.83	52.10	104.35	28.19	23.72
		16.65	104.59	84-569*-12R-6, 14–20 cm		4.68	74.54	0.22	0.86	9.56	38.65	65.90	43.22	21.07
S24	Ilopango	17.02	107.67	84-569*-13R-1, 97–102 cm		3.63	76.46	0.18	1.13		47.74	112.30	32.57	17.58
		17.42	199.30	67-494A-18R-1, 30–33 cm		3.68	76.85	0.11	1.11					
S25	Amatitlán	21.53	218.69	84-569*-24R-5, 59–60 cm		4.81	77.79	0.12	0.75	6.25	56.04	151.39	30.90	13.93
		21.92	209.04	67-494A-19R-1, 54–62 cm		4.31	77.46	0.09	0.71					

Note. CAVA = Central American Volcanic Arc.

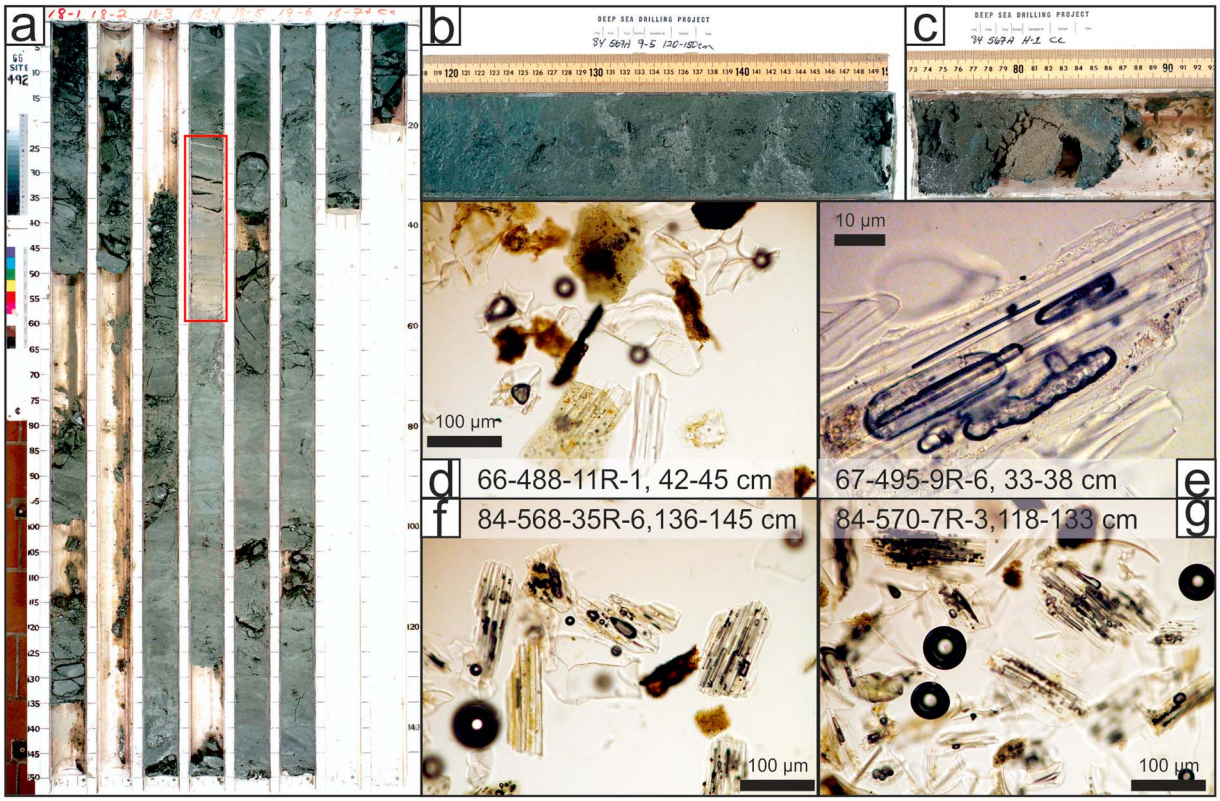

Figure 4. Images of marine drill cores (from www.iodp.tamu.edu) and smear slide pictures of exemplary tephras. (a) Highly disturbed Core 66-492-18R, drilled offshore Mexico. Red box highlights a thick primary tephra layer that is only slightly disturbed by drilling. (b) Biscuited Section 84-567A-9R-5. Lighter patches are remnants of a marine ash layer. (c) Core catcher Section 84-567-1R-CC with a brown ash layer. (d–g) Smear slide images of transparent, highly vesicular glass shards. Sample intervals are given in each image.

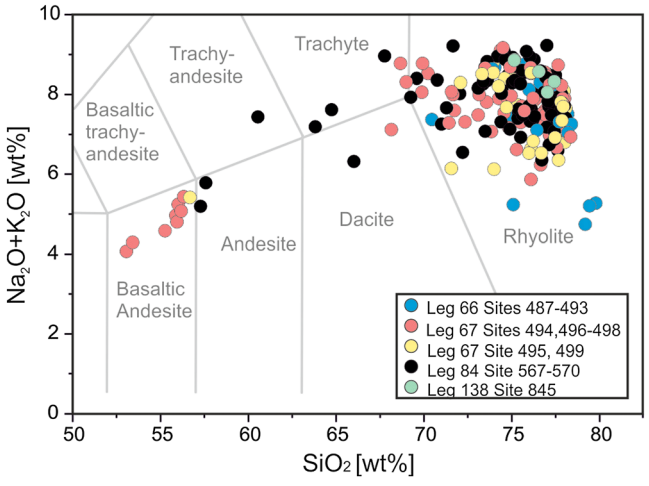

Figure 5. Total alkali versus silica plot to indicate compositional variability in tephras and to discriminate between volcanic rock classes after Le Maitre et al. (2002). Matrix-glass compositional ranges of marine ash beds (normalized to anhydrous compositions). Averages per sample; standard deviation within symbol size.

correlations between the sites of the last 450 ka are shown in Figure 11. Geochemical correlations to volcanic eruptions and volcanic complexes along the arcs are possible because of characteristic compositional variations from Nicaragua in the South to Mexico in the North (see section 2). We use a large geochemical database derived from literature and own data to establish multiple provenance and correlation diagrams to correlate the marine tephra layers to known eruptions or allocate their provenance areas along the arcs (shown in Figures 6–10). In the following, we describe these correlations and/or source classifications with respect to their volcanic source areas from North to South.

4.2.1. Correlations to Mexico

Nineteen single ash beds from Sites 487 (# 3, 6, and 9), 492 (#2, 4, 5, 7, and 8), 493 (#1, 10, 11, and 12), 495 (#14, 22, 29, and 33), 497 (#6 and 13), and 498 (#5) probably originate from the Mexican volcanic arc and cover the age range from Pleistocene to Middle Miocene with a maximum age of ~15 Ma (Figure 12). Tephra layers from the TMVB are characterized by, for example, high La/Yb (>10) and in general low Ba/Zr (<10; Figures 9 and 10). The along arc provenances of these tephra layers indicate volcanic sources similar to Popocatépetl and the Las Cumbres Volcanic complexes in the western part of the TMVB (Figure 10). Additionally, two ash beds from sites offshore Mexico, associated to volcanic sources in Mexico, can be correlated to sites offshore Guatemala (*S16* and *S18*; Figures 8 and 9; Table 4). Tephra layer *S16* (Sites 493, 492, and 568) is ~4.8 Ma and *S18* (Sites 492 and 569) ~8.2 Ma old.

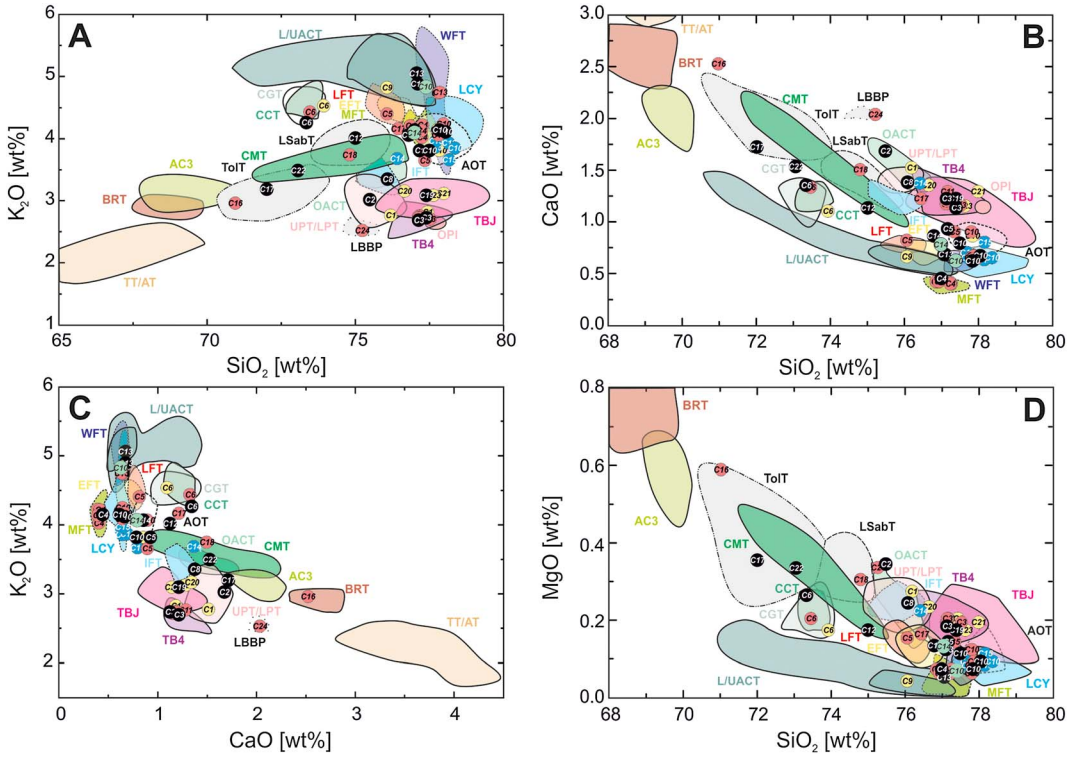

Figure 6. Correlations *C1–C24* to known deposits on land. (a–d) Major element glass shard compositions of marine ash beds compared with proximal glass-composition fields of North-Central American Volcanic Arc tephras after Kutterolf, Freundt, Peréz, et al. (2008), Kutterolf, Freundt, & Peréz (2008), Kutterolf, Freundt, Schacht, et al. (2008), Kutterolf, Liebetrau, et al. (2008), and Kutterolf et al. (2016). For clarity, data are averages of all analyses made for each tephra. Color code for marine sites is the same as in Figure 5. Abbreviations of tephra deposits are the same as in Figure 3. Averages per sample; standard deviation within symbol size.

4.2.2. Correlations to Guatemala

4.2.2.1. Atitlán-St. Maria Formation

Deposits from the Atitlán-St. Maria Formation are characterized by, for example, high Ba/Zr (up to 25), very high Rb/Hf (up to 70), and La/Yb ratios (~8–17) but low Zr/Nb ratios (<25) (Figures 8 and 9). The tephra layer *C8* recovered at site 569 may be correlated to the I-Fall Tephra (IFT; Figure 6). Koch and McLean (1975) estimated the I-Fall as >40 ka old; we determine an age of ~54 ka for tephra layer *C8*. Tephra layer *C10* is the 84-ka-old Los Chocoyos Tephra (LCY), and we found the marine deposits of this large eruption in the sediment record of Sites 487, 494, 496, 497, 499, 568, 570, and 845 (Figure 11). Correlation is based on the typical major element glass geochemistry, for example, high SiO_2 (77.7–78.4 wt%), low CaO (~0.65 wt%), and FeO concentrations (~0.65 wt%) as well as distinctively high Ba/La ratios (>60) at low Zr/Nb ratios (<15; Figures 6 and 7; Table 3). The LCY eruption generated a very widespread tephra layer that is not only found offshore Guatemala but also offshore Mexico (site 487) as well as 600 km away from the Pacific coast at site 845. This agrees with the observation of studies in the Gulf of Mexico and elsewhere that found the marine equivalent of this eruption at large distances between Florida and Ecuador (e.g., Drexler et al., 1980; Kutterolf, Freundt, Peréz, et al., 2008; Kutterolf et al., 2016; Ledbetter, 1985).

Tephra layer *C13* correlates with the 158-ka W-Fall Tephra (WFT; Sites 496, 497, 567, and 568; Figure 11), characterized by high K_2O (typically around ~5 wt%) and silica contents (77–78 wt%) as well as the highest La/Yb ratio (14–20) in Northern CAVA tephras (Figures 6 and 7; Table 3). Tephra layer *C15* (Sites 487 and 488; Figure 11) is the Atitlán Older Tephra, which is probably ~306 ka old (Figures 6 and 7; Table 3) and shows the same compositional signature as Los Chocoyos but can be distinguished by its stratigraphic position. This tephra has been found in the lake sediments of Lake Petén Itza in Northeast Guatemala as well as in some Pacific gravity cores offshore El Salvador (Kutterolf, Freundt, Peréz, et al., 2008; Kutterolf et al., 2016).

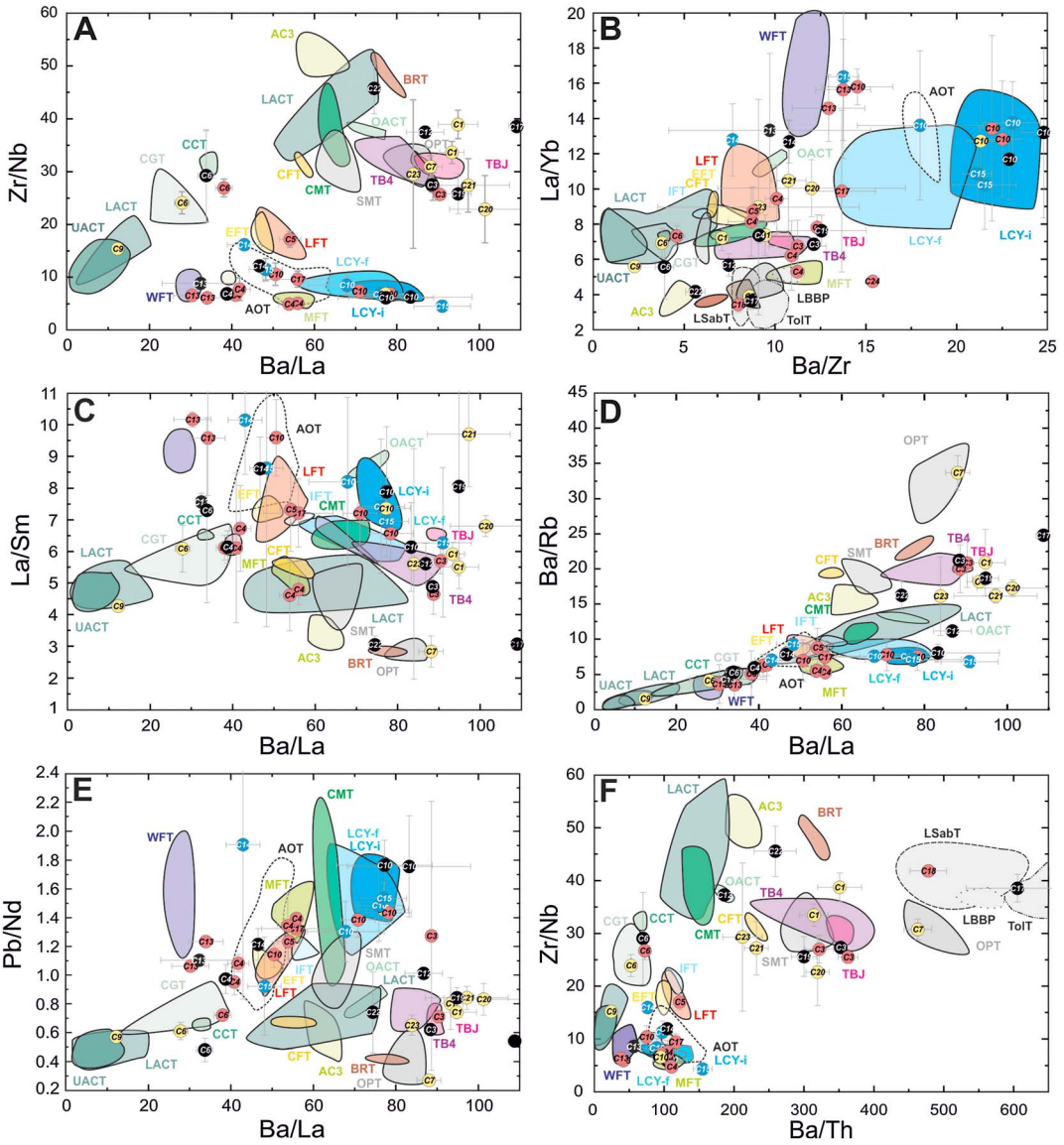

Figure 7. Correlations *C1–C24* to known deposits on land. (a–f) Average trace element ratios of glass shard compositions of marine ash layers. Trace element correlation fields for known eruptions from Guatemala and El Salvador after Kutterolf, Freundt, Peréz, et al., (2008) and Kutterolf et al. (2016). Abbreviations of tephra deposits are the same as in Figure 3. Standard variations per analyzed tephra are shown with gray bars. Color code for marine sites is the same as in Figure 5.

The two tephra layers *S6* (0.51 Ma; site 494) and *S7* (~0.57–0.54 Ma; Site 494) are correlated with marine ash beds from gravity cores taken during Meteor cruise M66 (core M66-230 offshore El Salvador) and contain the high Ba/Zr (~13) and Rb/Hf (55) ratios that are characteristic for eruption products from Atitlán Caldera (Figures 8 and 9; Table 4). Tephra layer *S19*, with similar trace element compositions, is correlated between Sites 567 and 568 and associated with an eruption from Atitlán at ~13.9 Ma. Tephra layer *S21* (~14.4 Ma; Sites 568 and 569) has a bimodal composition at Site 569 indicating a mix of Guatemalan and El Salvadorian ash (Figures 8 and 9; Tables 4 and S1).

Two single ash beds at Sites 497 (#2) and 569 (#3) can be compositionally associated with eruptions from Atilán Caldera at 414 and 421 ka. Three single ash beds at Site 570 (#19; 2.76 Ma) and site 845 (#1; ~2.45 Ma) are also associated with Atitlán Caldera. Four single ash beds in the Miocene sediments of Sites 495 (#42; 11.9 Ma), 568 (#40; 15.4 Ma; #43; 15.5 Ma), and 569 (#49; 22.4 Ma) are geochemically similar to the WFT and therefore probably associated with an old eruption from Atitlán (Figures 8 and 10; Table S1).

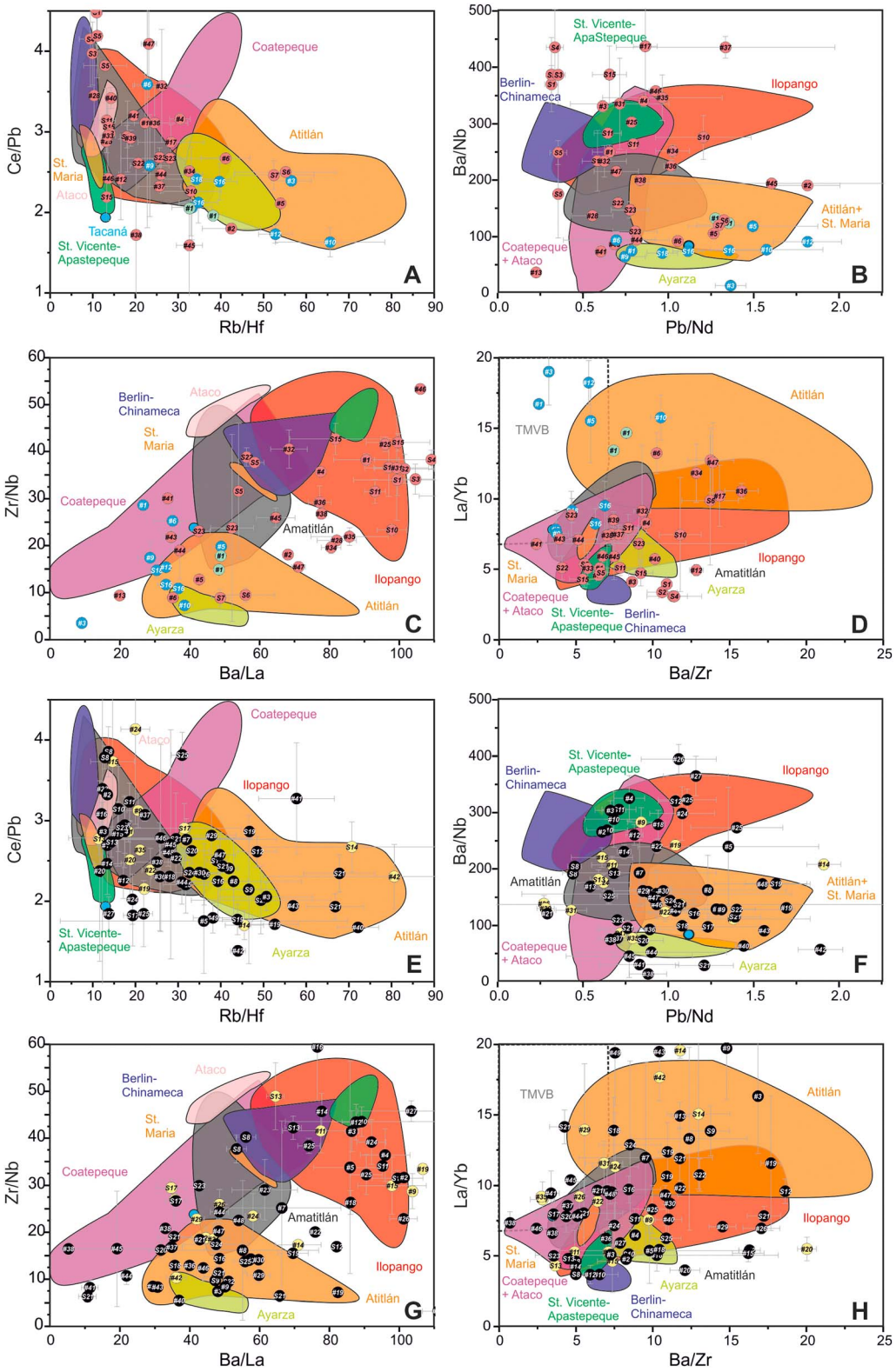

Figure 8. Correlations of site-to-site correlations (*S1–S25*) and all remaining single ash beds (#) to volcanic complexes of Guatemala and El Salvador. Trace element ratios of glass shard compositions. (a–d) Marine tephras of Sites 487, 488, 492, and 493 offshore Mexico and incoming plate Sites 495 and 499 offshore Guatemala. (e–h) Marine tephras from slope Sites 567, 568, 569, and 570. Standard variations per analyzed tephra are shown with gray bars. Color code for marine sites is the same as in Figure 5.

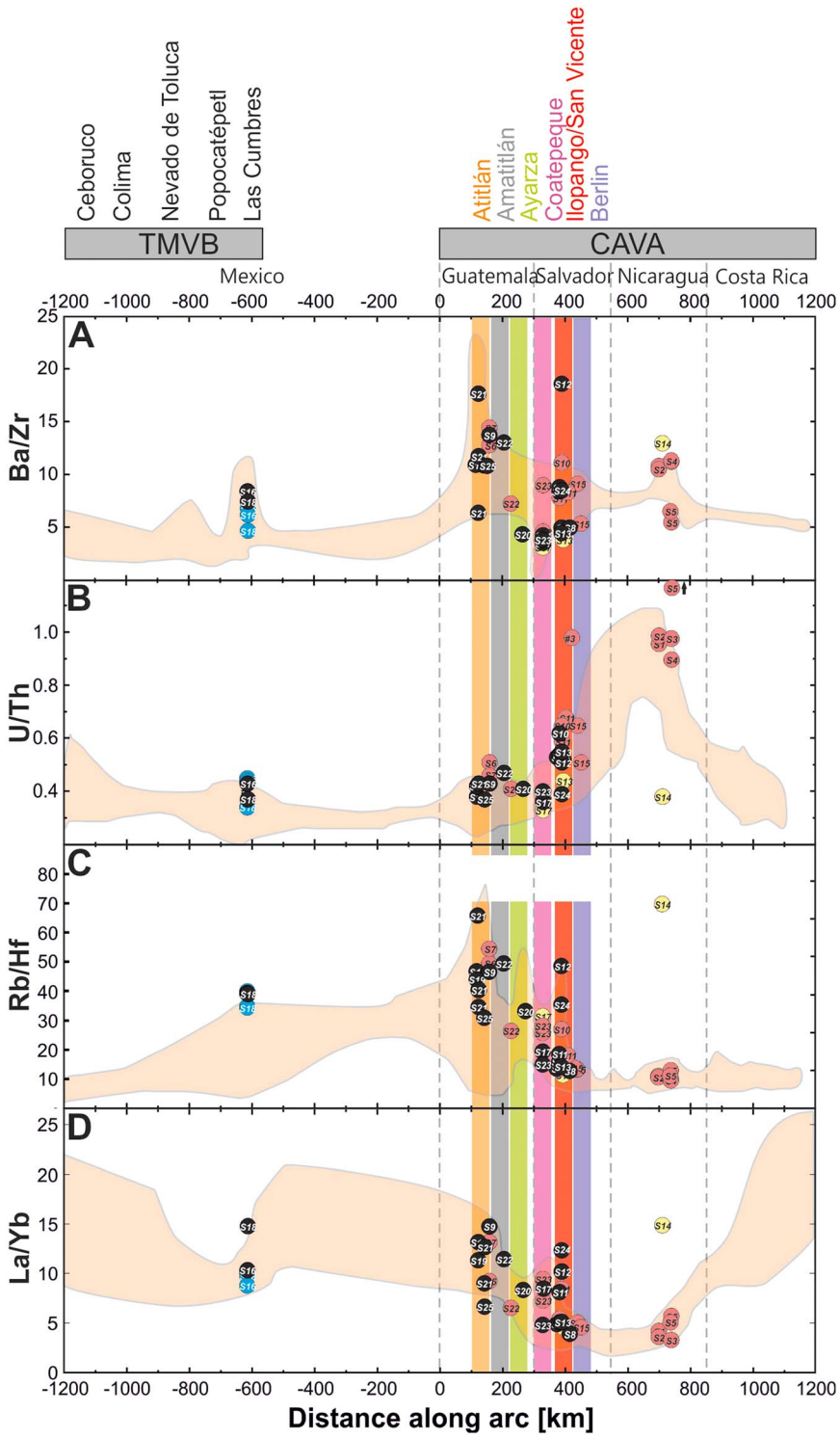

Figure 9. Comparison of average glass compositions of marine ash layers that can be correlated between several sites (*S1–S25*) with Ba/Zr, U/Th, Rb/Hf, and La/Yb variations along the CAVA and Mexican arcs as discussed in the text. Modified after Kutterolf et al. (2016). Along-arc variations of CAVA are based on corresponding felsic and mafic ratios as well as glass and bulk rock compositions (Carr et al., 2007; Kutterolf et al., 2016). Mexican compositional fields are only based on bulk rock data, given in Luhr et al. (2006), but are assumed to provide the same provenance information. Positive distances along the arc represent CAVA provenances; negative distances along the arc indicate Mexican origin. Color code for marine sites is the same as in Figure 5. TMVB = Trans Mexican Volcanic Belt; CAVA = Central American Volcanic Arc.

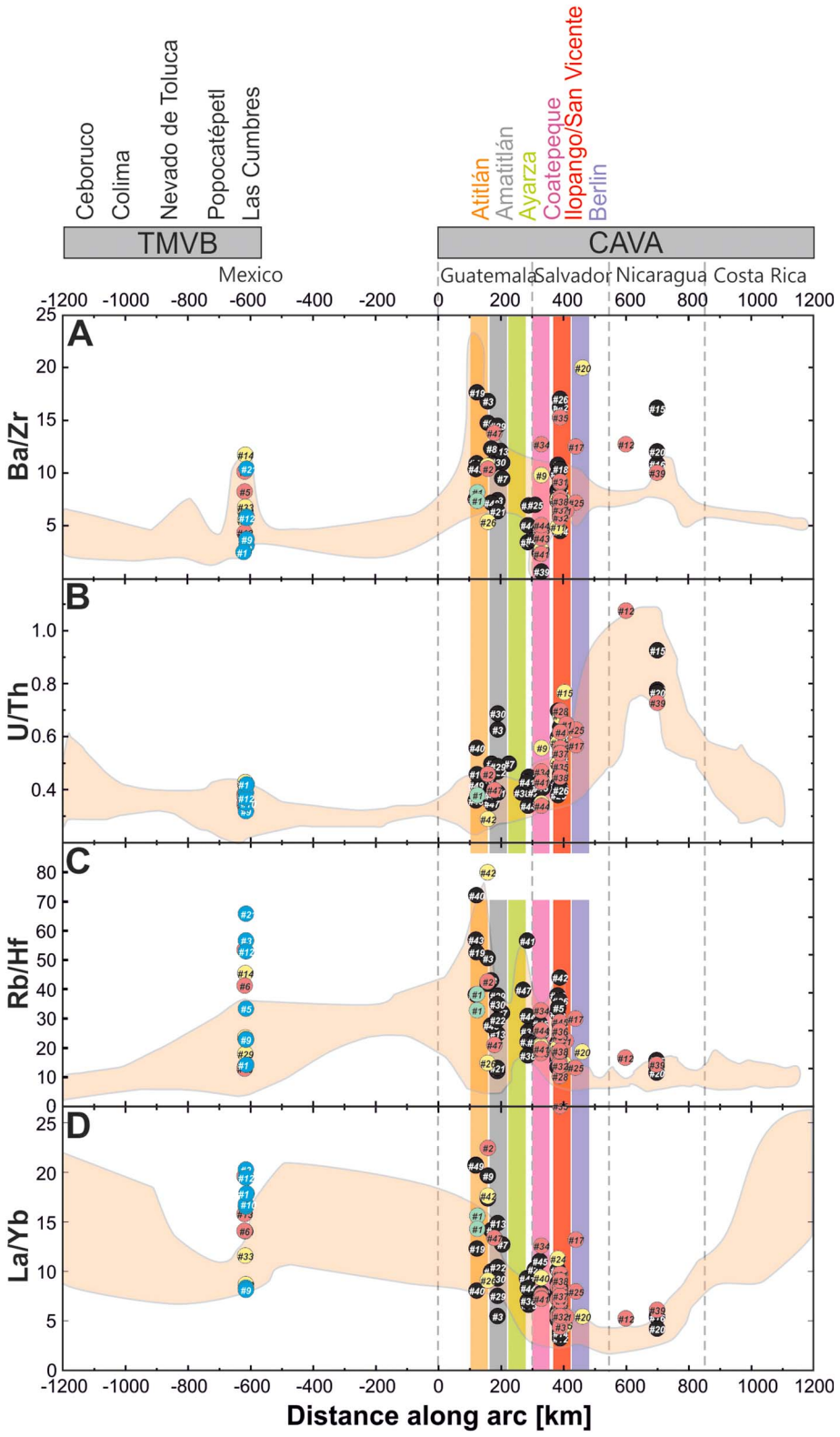

Figure 10. Comparison of average glass compositions of single marine ash beds (#x) with Ba/Zr, U/Th, Rb/Hf, and La/Yb variations along the CAVA and Mexican arcs as discussed in the text. Modified after Kutterolf et al. (2016). For further information see Figure 9. Color code for marine sites is the same as in Figure 5. TMVB = Trans Mexican Volcanic Belt; CAVA = Central American Volcanic Arc.

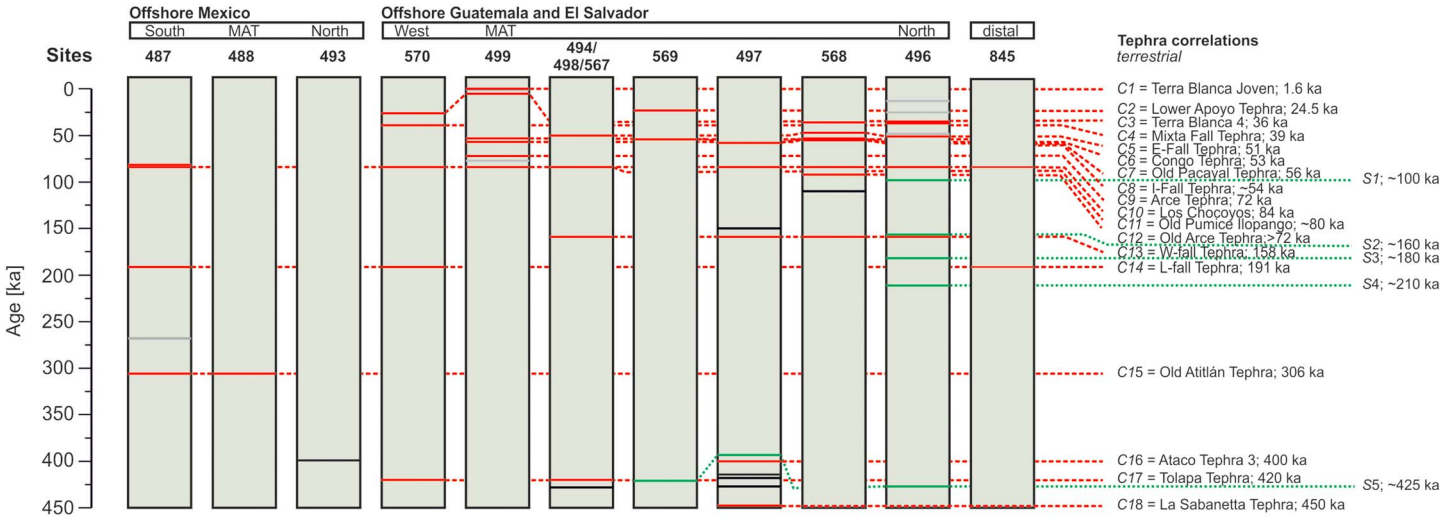

Figure 11. Compositionally correlated tephra layers of the last 450 ka. Tephra layers *C1* through *C18* provide chronostratigraphic links between the drill sites offshore northern Central American Volcanic Arc and Mexico. Sites are arranged from South (right) to North (left) offshore Mexico and from West to North offshore Guatemala and El Salvador. Site 845 is more distal (~600 km) offshore Guatemala. Layers *C1* to *C18* (red) correlate with specific tephras on land as shown in Figures 6 and 7 and Table 3. Layers *S1–S5* (green) are correlated between the sites and to source regions on land (see Table 4). Unlabeled ash beds could not be correlated between sites or to known eruptions on land (black). MAT = Middle American Trench.

4.2.2.2. Amatitlán-Antigua Formation

The Amatilán-Antigua Formation is characterized by, for example, Zr/Nb ratios >15, Ba/La ratios between 40 and 70, and high Rb/Hf ratios <40 (Figures 8 and 9). Tephra layer *C5* is the 50-ka E-Fall Tephra that was recovered at Sites 496, 498, and 568 (Figure 11). This correlations is based on the typical glass composition with high SiO_2 concentrations (~76–77 wt%) and CaO contents of ~0.9 wt% but especially on the specific trace element compositions (e.g., Ba/La ~45–55; Zr/Nb ~15–20; Figures 6 and 7; Tables 3 and S1). The marine deposits of the 191-ka L-Fall Tephra were found offshore Guatemala but also offshore Mexico at Sites 487, 570, and 845 (*C14*; Figures 6 and 7). Both E-Fall and L-Fall Tephras have high potassium contents (>4.4 K_2O wt%), contain biotite, and are also deposited in the Gulf of Mexico (Kutterolf et al., 2016; Rabek et al., 1985), which illustrates their wide distribution and large eruption magnitude. Although E-Fall and L-Fall Tephras have very similar glass compositions, it is possible to distinguish them by their relative stratigraphic position relative to LCY (84 ka).

Two tephra layers (*S22* and *S25*) can be correlated between sites 569 and 494 offshore Guatemala (Figures 8 and 9; Tables 4 and S1), are Miocene in age (~15.8 and ~21.5 Ma), and are geochemically similar to Amatitlán (high SiO_2 ~77.5–78 wt%; high K_2O ~4.5–5 wt%; Rb/Hf ~27–49).

Ten single ash beds from Sites 568 (#44; ~15.6 Ma), 569 (#8, 13, 47, and 48; ~1.19, 1.33, 21.5, and 21.7 Ma L-Fall Tephra), 570 (#21, 22, 29, and 30; 3.49, 4.19, and 6.63 Ma), and 494 (#47; 22.1 Ma) are also compositionally correlated to the Amatitlán-Antigua Formation (Figures 8 and 10).

4.2.2.3. Ayarza Formation

Deposits of the Ayarza Formation have typically, for example, low Ba/Nb (<100) and Zr/Nb ratios (<10) and moderate high Rb/Hf ratios (>30). Tephra layer *C4* (Sites 496, 499, and 570; Figure 11) correlates with the chemical fingerprint of the 39-ka Mixta Fall from the Ayarza Caldera. The correlation is based on the distinctive major element composition with very low CaO (~0.4 wt%) and MgO (<0.1 wt%) contents at high K_2O (~4 wt%) and SiO_2 (~77 wt%) contents. Characteristic are the low Zr/Nb (<7) and Ba/Rb ratios (<7) at Ba/La ratios between ~40 and 60 (Figures 6 and 7; Tables 3 and S1).

Furthermore, we geochemically correlated an ash bed from Site 569 with an ash layer from the southern CAVA (tephra layer "s21" from Schindlbeck, Kutterolf, Freundt, Alvarado, et al., 2016), which is probably from an ~1-Ma eruption from Ayarza or Atitlán (tephra layer *S9*; Figures 6 and 7). Another correlation between sites 493 and 568 is tephra layer *S20* (14.5–14.3 Ma) that is geochemically similar to Ayarza but also has similarities with deposits known from Ataco Caldera (Figures 8 and 9; Tables 4 and S1).

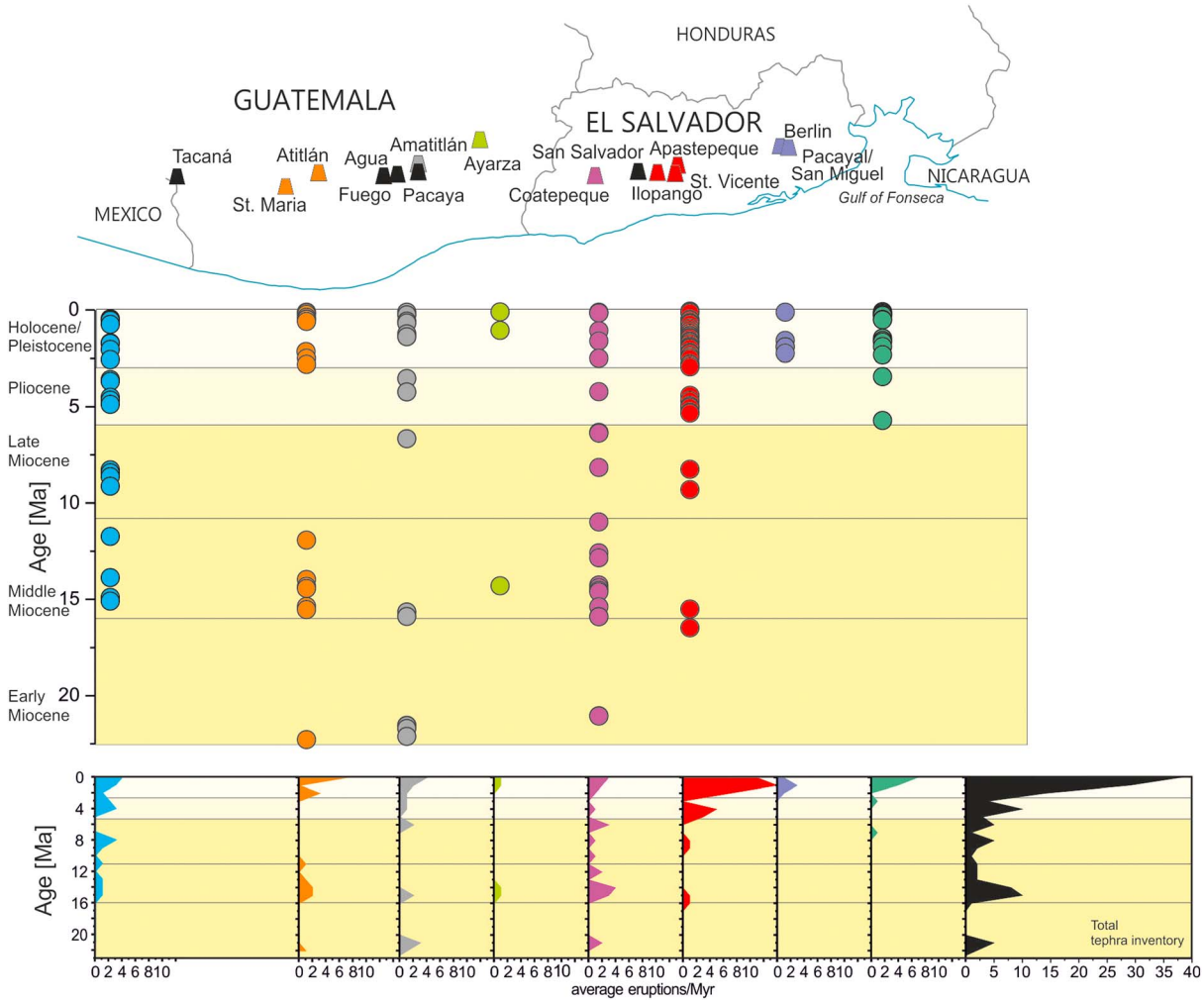

Figure 12. Distribution of marine tephra layers along the arcs over time. (a) Each colored circle represents a single eruptive event from the respective volcanic complex along the arcs; color code matches the colored major volcanic edifices in the upper panel; blue and dark green represents an origin from Mexico or Nicaragua, respectively. (b) Average number of tephras/eruptions per 1-Myr window to highlight episodes of increased explosive volcanic activity; the color code represents the volcanic complexes/arc segments as in (a). The black curve represents the total tephra inventory.

4.2.3. Correlations to El Salvador

4.2.3.1. Coatepeque-Ataco Formation

The Coatepeque-Ataco Formation covers a large geochemical range, but many eruptions have low Ba/La ratios (<60) and low Rb/Hf ratios (<40) but high Ce/Pb ratios (>2.5) and high potassium contents (K_2O > 3.5 wt%). Marine layer *C6* (Sites 497, 499, and 568; Figure 11) is compositionally equivalent to the 53-ka Congo Tephra from the Coatepeque Caldera, El Salvador. Deposits of the Congo Tephra are characterized by SiO_2 of ~74 wt% but high K_2O (>4.2 wt%) and CaO (>1.1 wt%) contents (Figure 6). Major element compositions overlap with compositions of the Conacaste Tephra, but trace elements (e.g., especially lower Zr/Nb <30) help to distinguish between these also temporally closely related eruptions. Additionally, we correlated marine tephra layer *C9* with the 72-ka Arce Tephras (L/UACT) and *C12* (Site 568) with the Old Arce Tephra (Figures 6 and 7). The correlation is supported by the high K_2O contents (4.8–5.5 wt%) as well as the exceptional low Ba/La (<20) and Ba/Zr (<7) ratios. Furthermore, tephra layer *C16* at Site 497 has the same major element composition as the ~400-ka Ataco Tephra 3 (Figure 6; Tables 3 and S1) with relatively low SiO_2 contents (~71 wt%) and ~3 wt% K_2O.

The older marine tephra layers *S17* (Sites 495 and 569; ~6.3 Ma), *S20* (Sites 493 and 568; 14.5–14.3 Ma), and *S23* (16.6–15.9 Ma) can be correlated between Sites 494, 496, and 569 (Figures 8 and 9; Tables 4 and S1) and also show the compositional characteristics of volcanic products from the Coatepeque/Ataco complex.

Furthermore, 17 single ash beds show the characteristic geochemical fingerprint known from the Ataco and Coatepeque Calderas (Table S1). Two ash beds from site 569 (#7 and #31; ~1 and 8.1 Ma) and one from site 497 (#32; 2.8 Ma) have the geochemical signature of the Ataco Caldera (Figures 8 and 10). Additionally, another four older single ash beds between 15.6 and 14.2 Ma are geochemically similar to the Ataco Caldera (#36, 37, 38, and 44 from Site 568). Ten single ash beds in the sediments offshore Guatemala can be correlated to the Coatepeque-Ataco Formation (Figures 8 and 10). Except tephra layer #9 (Site 499; 1.55 Ma), all of the other layers have been deposited in the Miocene (#34 [Site 497]; #40 [Site 495]; #41 [Site 498]; #43 and 44 [Site 496]; #39, 45, and 46 [Site 569]; and #41 [Site 568) between 21.1 and 6.3 Ma.

4.2.3.2. Ilopango and Apopa-Cojutepeque Formation

The Ilopango Formation is known for high Ba/La (>60), Ba/Zr (up to 20), and Zr/Nb ratios (>25) at moderate to high potassium and calcium contents (3 to 5 wt% K_2O, >~1 wt% CaO) for silica contents >76 wt% SiO_2 (Figures 6, 8, and 9). We correlate the Terra Blanca Joven (TBJ) eruption (1.5 ka) to a tephra in the uppermost centimeters of Site 499 (*C1*), as well as the 36-ka Terra Blanca 4 (TB4) eruption to tephra layer *C3* at Sites 496, 499, 568, and 570 (Figures 6, 7 and 11; Table 3). The correlations are based on the characteristic glass shard major and trace element compositions as well as the relative stratigraphic position in the cores. The deposits of TBJ and TB4 have relatively low K_2O (<3 wt%) at high SiO_2 (>76 wt%; Figure 6). Even more distinctive is the trace element composition with typically high Ba/Th ratios (>300) and high Ba/La ratios (>85; Figure 7; Tables 3 and S1). Marine tephra layer *C11* that was recovered at site 494 corresponds to the 80-ka Old Ilopango Tephra, which is supported by the stratigraphic position and the same major element signature as TBJ and TB4 eruption products (Figure 6; Table 3). Not so much is known about the older Pleistocene eruptions from Ilopango Caldera (Kwasnitschka, 2009), but we found the Feliz Tephra (*C19*; 0.66 Ma at Site 569), the Salvamex Tephra (*C21*; 1.03 Ma at Site 495), and the La Curva Tephra (*C22*; 1.15 Ma at Site 569) as marine equivalents in the sediments offshore Guatemala (Tables 4 and Table S7). These are the first age constraints for the older Ilopango succession exposed along the Pan American Highway North of the caldera (Kwasnitschka, 2009), which fills the gap between the Terra Blanca succession and ~2 Ma old ignimbrites South of the caldera.

Moreover, site-to-site correlated tephra layers *S8* (Sites 568 and 570; 0.6 Ma), *S10* (Sites 497 and 568; ~1.3 Ma), *S11* (Sites 495, 496, 497, and 568; ~1.6 Ma), *S12* (Sites 568 and 570; 2.2 Ma), *S13* (Sites 495 and 570; 2.32–2 Ma), *S15* (Sites 494 and 496; 3–2.9 Ma), and *S24* (Sites 494 and 569; 17.4–17 Ma) are probably from eruptions from the Ilopango area, assuming that magmatic compositions remained similar throughout that time span. However, tephra layer *S12* shows also some geochemical similarities with Atitlán (Figures 8 and 9; e.g., high Ba/Zr; Tables 4 and S1).

Additionally, there are at least 28 single ash beds (Figures 8 and 10) that can be compositionally attributed to older formations at Ilopango reaching back until ~16.5 Ma (Sites 499 [#10; 1.58 Ma]; 495 [#19; 1.92 Ma]; 496 and 497 [#3, 4, 28, 31, 35, 36, 37, 38, 45, and 46]; 845 [#2]; 499 [#11]; 568 [#23, 24, 25, 26, 27, and 42]; 569 [#2, 3, 4, 10, 11, 14, and 32]; and 570 [#5 and 18]).

4.2.3.3. St. Vicente-Apastepeque Formation

Eruptions from the St. Vicente-Apastepeque Formation are geochemically similar to the Ilopango Fomation but have in general lower Rb/Hf and La/Yb ratios (<15 and ~5, respectively; Figures 8 and 9). The Upper and Lower Apastepeque Pumice are the oldest known eruptions from the St. Vicente-Apastepeque Formation on land, but no age constraints have been found so far (Figure 3). We probably found the marine deposits of both eruptions in the sediments of site 499 applying compositional fingerprinting (tephra layers *C20* and *C23*; Figure 6). The Apastepeque Pumice on land has silica contents of ~76 wt% with lower K_2O contents (2.8–3.1 wt%) but higher FeO (1.5–1.6 wt%) and CaO (1.4–1.6 wt%) contents (Figure 6). The calculated ages for these eruptions are ~0.88 and ~1 Ma. Additionally, one single ash bed at Site 495 (#15; 1.81 Ma) can probably be associated with an even older eruption from this volcanic complex.

4.2.3.4. Berlin-Chinameca Formation

The Berlin-Chinameca Formation is the southernmost tephra formation in El Salvador and geochemically characterized by, for example, low Pb/Nd (<0.5) and low Rb/Hf (<12) but high U/Th (0.4–0.8) and Zr/Nb (>30) ratios (Figures 8 and 9). Tephra layer *C7* correlates to the Berlin-Chinameca complex and specifically to the 56-ka Old Pacayal Tephra, which Kutterolf, Freundt, Peréz, et al. (2008) and Kutterolf et al. (2016) also found as a marine tephra in gravity cores of RV Meteor cruise M66 and as an ash layer in sediments of Lake Petén Itza. Next to its compositional similarity (~57 wt% SiO_2; very high Ba/Th ~460 and Ba/Rb >30), *C7* also

fits into the relative stratigraphic order known from previously studied onshore, lacustrine, and marine sediments in this region (Figures 7 and 11; Table S1).

There are additionally four single ash beds identified at Site 494 and one at site 495 that are geochemically similar to the Berlin-Chinameca Formation but also show some similarities with the St. Vicente-Apastepeque Formation (Figures 8 and 10). These tephras were deposited between 1.5 and 2.2 Ma (#8, 16, 17, and 25; Site 494 and #20; Site 495).

4.2.4. Correlations to Nicaragua

Typical for the Nicaraguan part of the CAVA is geochemical compositions with very high Ba/La (up to 140) and Ba/Th (>400) ratios but very low Rb/Hf ratios (<10) (Figures 8 and 9). Tephra layer *C2* is correlated with the 24.5-ka Lower Apoyo Tephra, product of a Plinian eruption from Apoyo caldera in Nicaragua, which has very specific potassium, iron, magnesium, and calcium contents at high silica values compared to other CAVA tephras in this age range. Kutterolf, Freundt, Peréz, et al. (2008) used these compositional characteristics to show that ash from the Lower Apoyo Tephra eruption has been dispersed westward across the Pacific, which fits our detection of layer *C2* at Site 569.

The Malpaisillo Caldera in Nicaragua has produced several large eruptions. In the cores offshore Guatemala, we correlate the 420-ka Tolapa Tephra (*C17*; Sites 494 and 570) and the 450-ka La Sabanetta Tephra (*C18*; Site 497) to ash layers in the sediments offshore Guatemala. The correlations are based on major and trace element glass compositions (Figures 6a, 6b, 6d, 7b, and 7f), whereby the very high Ba/Th (>400) and Ba/La (>110) ratios of the Malpaisillo rocks are particularly helpful. Additionally, tephra layer *C24* can be assigned to the Lower Boulevard Bio Pumice (Site 494; 1.8 Ma) originated from an unknown source in Central Nicaragua, with typically high CaO (~2–3 wt%) at low K_2O (<2.7 wt%) contents (Figures 6a–6c, 7b, 7f and 11; Tables 3 and S1).

Furthermore, we correlated several, mostly mafic, tephras from Nicaragua between marine sites that suggest an origin from the Masaya/Las Sierras volcanic complex in central Western Nicaragua (Table S1). Tephra layer *S1* (0.1 Ma) is a correlation between Site 496 and a marine gravity core M66-223_69–76 cm (Kutterolf, Freundt, Peréz, et al., 2008). Tephra layer *S2* (0.16 Ma) can be correlated with tephra layer "s3" from Schindlbeck, Kutterolf, Freundt, Alvarado, et al. (2016), which is a widespread tephra that can be found in multiple ODP and IODP sites in the Pacific (Sites 1039, 1254, 1255, U1381, and U1414). Tephra layers *S3*, *S4* (0.18 and 0.21 Ma; Site 496), and *S5* (~0.4 Ma; Sites 496, 497, and 569) can be correlated to marine tephra layers from Sites 1242 and U1381 offshore Costa Rica (tephra layer "s10" from Schindlbeck, Kutterolf, Freundt, Alvarado, et al., 2016). The 2.26-Ma felsic tephra layer *S14* can be found in the sediments of Sites 495 and 1039 offshore Costa Rica (Figures 8 and 9; Table 4); this tephra layer might originate from the Tertiary Coyol arc (Ehrenborg, 1996) in the highlands of Nicaragua, 100 km east of the modern Nicaraguan arc (Schindlbeck, Kutterolf, Freundt, Alvarado, et al., 2016).

Additionally, five single felsic ash beds from Sites 497 (#12 and 39; 1.6 and 5.7 Ma, respectively), 569 (#15 and 16; 1.39 and 1.52 Ma, respectively), and 570 (#20; 3.39 Ma) probably originated from Nicaraguan eruptions as well, as respective provenance diagrams indicate (Figures 8 and 10).

5. Implications for North Central American Volcanism

To understand the temporal evolution of the explosive volcanism in Central America as well as the evolution and distribution of specific eruptions, it is necessary to study a long and most complete record. The major problem on land is the lack of outcrops of old deposits due to extensive erosion and successive coverage by younger deposits. Even more complicated are relative age estimates in case of missing stratigraphic relationships. The marine tephra record provides the opportunity (1) to extend and complete the record of explosive eruptions for the individual volcanic centers and regions along the arcs and (2) to build a temporal framework using the age estimations derived from marine sedimentation rates.

5.1. Age Implications for Terrestrial Eruptions

We obtained eight new ages for already known but so far undated eruptions from Nicaragua, El Salvador, and Guatemala. Our dating of the IFT to ~54 ka by correlation to marine tephra layer *C8* at Site 569 (Figures 6, 7, and S1) also defines the time when the period of huge explosive eruptions from Atitlán caldera ended. This caldera thus produced its nine large-volume widespread tephras from 158 to 54 ka.

The recent eruptive history at Ilopango Caldera is recorded in the well-known Terra Blanca Tephras (<36 ka; Kutterolf, Freundt, Peréz, et al., 2008). The underlying thick and complex tephra succession has been stratigraphically logged by Kwasnitschka (2009), but the only age constraint is the ignimbrite (1.77 ± 0.22–1.81 ± 0.22 Ma; Lexa et al., 2011) below an unconformity at the base of the sequence. We found three tephras of that succession in the marine cores at 0.66, 1.03, and 1.15 Ma (layers *C19*, *C21*, and *C22*, respectively). The respective tephra beds (Feliz Tephra, Salvamex Tephra, and La Curva Tephra) belong to the Cojutepeque unit of Kwasnitschka (2009), which is overlain by the Soyapango (seven tephras) and Apopa (five tephras) units (Figure 3). The new ages imply that the Soyapango and Apopa tephras were emplaced between <660 and >36 ka and that tephras below the Cojutepeque unit (>1.15 Ma) are associated with the older ignimbrite succession.

The previously undated Upper and Lower Apastepeque Pumice tephras (>2 m thick each) from Apastapeque Caldera were erupted at of ~0.88 and ~1 Ma as inferred from correlation to marine tephra layers *C20* and *C23*. They are thus much older than we had previously assumed (cf. Figure 3) and imply a considerable time gap between Apastepeque caldera and St. Vicente volcanic activity.

For Nicaragua, the ~450-ka age of La Sabanetta Tephra, correlated to layer *C18* (Site 497), fits the results from the recent study of the Malpaisillo Formation by Stoppa et al. (2018), who radiometrically dated the directly overlying Tolapa tephra (420 ± 40 ka) and the 570 ± 70-ka-old La Paz Centro Tephra at the base of the Malpaisillo Formation (Stoppa et al., 2018).

Finally, the Boulevard Bio Pumice obtains the ~1.8-Ma age of marine tephra layer *C24* (Site 494). This age suggests its origin from the late stages of the Tertiary Coyol arc in Central Nicaragua.

5.2. Temporal Evolution of Explosive Volcanism Along the Arcs

The investigated marine tephra record offers the opportunity to study the history of the explosive eruptions from the different regions and volcanic complexes along the arc back in time. In Figure 12, the temporal distribution of eruptions is shown along the arc; each tephra is associated with the respective volcanic complex/region that we have assigned by geochemical correlations.

Newhall (1987) postulated three caldera stages (11 Ma, 8 Ma, and 84 ka) for the Atitlán volcanic complex. The marine tephra layers between ~14–12 and >21 Ma are probably associated with eruptions from the first Atitlán stage or an even older, previously not recognized stage. However, we do not see any evidence for explosive eruptions from the second stage (8 Ma) in the marine cores. Stage three comprises nine major eruptions from 158 to 54 ka (WFT to IFT) of which the extremely voluminous Los Chocoyos eruption (84 ka) was a main caldera forming event. However, new observations on dispersal characteristics yield large volumes also for other events; for example, the ~0.16-Ma WFT tephra has an updated erupted volume of ~90-km^3 DRE (dense rock equivalent) (Kutterolf, Freundt, Peréz, et al., 2008; Kutterolf et al., 2016). Hence, the third Atitlán Caldera may not have formed by the LCY eruption alone (Newhall, 1987; Rose et al., 1987) but may represent a nested caldera with subsidence phases at least after each of the large WFT and LCY eruptions. Moreover, marine ash layers at around 300 ka (*C15* = Atitlán Older Tephra) and around 500–600 ka (*S6* and *S7*) document large explosive eruptions at Atitlán preceding the main stage three.

The eruption record from the Amatitlán volcanic complex reaches continuously back until ~7 Ma (Figure 12), which is much longer than previously known from land. Koch and McLean (1975) described the R-tephra as representing at least five old (>0.5 Ma) eruptions from Amatitlán Caldera. However, we have found evidence for activity in the Amatitlán area during the Middle (~16–14 Ma) and Early Miocene (~23–21 Ma), at similar times as for Atitlán Caldera as well as for the Coatepeque and Ilopango calderas in El Salvador (Figure 12).

The Coatepeque/Ataco volcanic complex is the only one that has a more or less continuous record of tephras in the marine cores reaching back into the Early Miocene. However, this might represent a sampling bias since the region around the Coatepeque Caldera is the closest to many drill sites (~160 km; Legs 67 and 84), which might favor the preservation of smaller explosive eruptions in the marine sediments.

There are abundant marine tephras that originate from the Ilopango region (~200 km to legs 67 and 84), especially during the last ~6 Myr, but volcanism was also active during the Late (10–8 Ma) and Middle (16–14 Ma) Miocene (Figure 12). Explosive eruptions associated with the Berlin-Chinameca complex, however, are limited to the last ~3 Myr (Figure 12).

Several correlations to the mafic Las Sierras Formation in Western Nicaragua assist the longevity of the associated magmatic system over at least the last 400 kyr as it has been proposed by Schindlbeck, Kutterolf, Freundt, Alvarado, et al. (2016) and Schindlbeck, Kutterolf, Freundt, Straub, et al. (2016).

The eruption records derived from the marine deposits indicate a long history of explosive volcanism for the major volcanic complexes reaching back into the Early Miocene (Figure 12). However, for Nicaragua (and partly Honduras), where slab rollback caused a trenchward shift in the position of the volcanic front, the older Tertiary tephras must derive from volcanoes at the now extinct Coyol arc (Ehrenborg, 1996). Yet the geochemical characteristics of these tephras are very similar to those of tephras from the Quaternary volcanic front (Jordan, Sigurdsson, Carey, Lundin, et al., 2007; Nyström et al., 1988). This suggests that, despite the rollback, subduction conditions controlling magmatic compositions did not change much over the last 25 Myr.

5.3. Global Episodes of Enhanced Volcanic Activity

At the bottom of Figure 12, we show how the frequency of large eruptions at the major volcanic centers varies over time. The interesting observation is that many centers share time intervals of increased activity. This suggests that there may be some process controlling eruption frequency that operates at a scale at least covering the entire subduction zone length. We thus also show a total frequency distribution over time for the entire subduction zone from Nicaragua to Mexico.

This distribution indicates five pulses of enhanced explosive volcanic activity (Figure 12): (1) a pulse during the Quaternary, (2) a Pliocene pulse between 6 and 3 Ma, (3) a Late Miocene pulse between 10 and 7 Ma, (4) a Middle Miocene pulse between 17 and 11 Ma, and (5) an Early Miocene pulse (ca. $>$21 Ma). Several authors postulated episodic volcanic activity in Central America (e.g., Kennett et al., 1977; Reynolds, 1980). Reynolds (1980) studied effusive and explosive eruption products and proposed three Neogene episodes of volcanism for Guatemala, El Salvador, and Honduras. He defined three major formations that extruded during the Middle and Late Miocene (Chalatenango Formation), during the Late Miocene to Pliocene (Bálsamo Formation), and during the Pliocene to Pleistocene (Cuscatlán Formation). Although the study of Reynolds (1980) lacked good age control of the studied deposits, the overall observation of episodic volcanism is probably correct and the pulses agree well with our findings.

The tephra record from Mexico covers eruptions from the Middle Miocene to the Holocene with gaps between ~13 and 10 Ma (only one eruption) and between 8 and 5 Ma. This might either feature a real decrease in explosive volcanism or a sampling and preservation problem. Ferrari et al. (1999) postulated that volcanism in Mexico occurs in pulses with peaks between 31–28, 23, 10.5–9 Ma, and since 5 Ma. Indeed, we also see an increase in eruption frequency between 10 and 8 Ma and since 5 Ma (Figure 12).

Several studies postulated that volcanic activity occurs in episodes (e.g., Kennet & Thunell, 1975). Comparing our data with published pulses in volcanic activity at different regions around the ROF (ring of fire) and with global climate and tectonic events indicates some temporal coincidences (Figure 13).

Kennett et al. (1977) were the first to describe two major pulses at 2–0 and 16–14 Ma, as well as two less pronounced periods of enhanced effusive and explosive volcanism between 6–3 and 11–8 Ma for the Southwest Pacific, Central America, and the Cascades (Figure 13). The same pulses were also recognized in a tephra compilation from several DSDP sites and especially in Legs 66 and 67 (Cadet, Pouclet, et al., 1982; Cadet, Thisse, et al., 1982; Kennett et al., 1977; Kennett & Thunell, 1975). Marine tephra records from Japan indicate similar periods of increased explosive volcanic activity between 2–0, 6–4, ~8, and possibly 15–13 Ma (Mahony et al., 2016; Figure 13). In the Caribbean, Carey and Sigurdsson (2000) and Sigurdsson et al. (2000) studied the temporal distribution of ash beds at several ODP sites. They found periods of enhanced ash accumulation in the marine sediments of ODP Leg 165 during the Late Miocene (~11–7 Ma) and the Early to Middle Miocene ($>$12 Ma) as well as during the Oligocene and Eocene (Figure 13). Sigurdsson et al. (2000) already noted that their Late Miocene and Early–Middle Miocene peaks agree with results of Kennett and Thunell (1977), Cadet, Pouclet, et al. (1982), and Cadet, Thisse, et al. (1982) although with a small temporal offset. The pronounced Quaternary and Pliocene peaks, however, were not detected in the Caribbean tephra records (Figure 13). Our Pacific Central American record does, however, support all periods of enhanced eruption activity at $<$2, 3–6, 7–10, and 11–17 Ma and thus agrees with other regions around the ROF, allowing for some minor deviations in individual lengths of episodes.

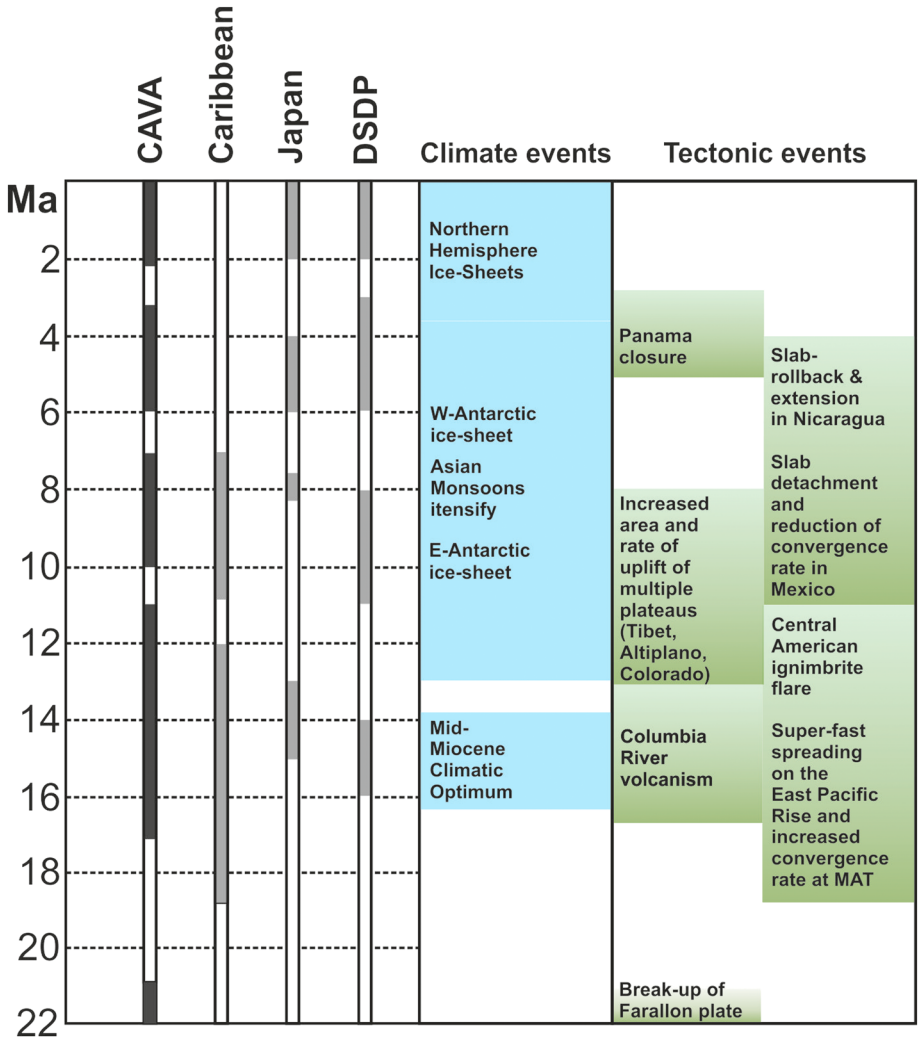

Figure 13. The temporal relationship of Neogene and Quaternary episodes of high volcanic activity and tectonic and climatic events. Episodes of increased volcanism of Central America (CAVA) from this study. Caribbean data from Sigurdsson et al. (2000) and Carey and Sigurdsson (2000). Episodes of increased volcanism of Japan after Mahony et al. (2016). Data compilation of the SW Pacific, Central America, Cascades after Kennett et al. (1977). Climatic and tectonic events after Zachos et al. (2001), Rogers et al. (2002), Mann et al. (2007) and Ferrari (2004). CAVA = Central American Volcanic Arc.

Possible causes for these pulses of enhanced volcanic activity are thought to be related to changes in large-scale plate tectonics (e.g., Mahony et al., 2016) or to climate influencing the lithospheric regime by suppressing or favoring magma ascent (e.g., glacial loading and unloading; e.g., McGuire et al., 1997; Rampino et al., 1979) or by affecting erosion and sedimentation rates. For example, Sigurdsson (1990) attributed variations in marine sedimentation rates to changes in atmospheric circulation due to climate changes. Von Huene and Scholl (1991) suggested that a larger amount of subducted sediments during the Quaternary led to an increase in arc volcanism over the last 2 Myr.

While our data cannot constrain any physical processes, we do observe some temporal coincidences between tectonic, climatic, and volcanic events globally.

1. The breakup of the Farallon into the Cocos and Nazca plates at about 23 Ma and subsequent rearrangements in the subduction zone caused large-scale topographic uplift and extension in northern Central America (Mann et al., 2007), which may have enhanced volcanism. Additionally, this is also the time of superfast spreading on the East Pacific Rise, which lead to an increase in the convergence rate at the MAT. The Mid-Miocene pulse in volcanism also coincides with the peak in the Columbia River flood

basalt volcanism associated with widespread extensional tectonics in western North America (Kohn & Fremd, 2008), which indicates tectonic rearrangements along the Pacific-American boundary. The rapid rise of orogenic plateaus during this period (e.g., Tibetan Plateau and Himalaya), probably associated with changes in global plate tectonics, induced changes in global climate (Kohn & Fremd, 2008). For instance, the Mid-Miocene climatic transition from optimum to disrupted conditions influenced bioproductivity and therefore character and amount of sedimentation on the down going plates along the ROF that may have influenced the magma generation at the arc systems ROF-wide. The Mid-Miocene transition also marks the beginning of the interplay of cold and warm periods due to orbital forcing (Holbourn et al., 2005), which may have influenced the volcanism in the Mid-Miocene.

2. During the period of high volcanic activity between 10 and 7 Ma, northern Central America was bracketed between tectonic events in the north and in the south. In Mexico, the 11.5–6-Ma period of eastward migrating intense volcanism followed the eastward propagation of a slab tear that ultimately led to slab detachment and reduction of convergence rates (Ferrari, 2004). In Nicaragua, slab rollback from 10 to 4 Ma caused associated extension (Mann et al., 2007). In the global perspective, the 10 to 7 Ma intense volcanic period coincides with the Late Miocene global cooling (Herbert et al., 2016) and the onset of the Miocene reglaciation of the Antarctic ice sheet with global climatic consequences such as the intensification of the Asian monsoons (Ao et al., 2016). The episodic pattern of enhanced ice-rafted debris deposition during times of deglaciation provides evidence that the Late Miocene east Antarctic ice sheets underwent dynamic large size variations at orbital time scales (Grützner et al., 2003), implying periodic changes in isostatic loading of the ocean plates and the continents, but also the respective sedimentation (dust) on the ocean crust.
3. The episode between 6 to 3 Ma coincides with the proposed closure of the Panama isthmus associated with changes in plate direction and velocities possibly affecting magma generation at the Central American arc. This coincidence may be questionable since the exact timing of the closure is still under debate and the Caribbean volcanic record, close by, does not show this pulse.

In summary, it seems that there is an interplay of tectonic and climatic forcing on the volcanic systems at the ROF or even globally that controls the activity on long timescales, but further studies are needed to understand the physical mechanisms.

6. Conclusions

We provide a stratigraphically classified tephra database of glass compositions of large-magnitude Quaternary to Neogene explosive eruptions at Central America, together with correlations of marine tephra layers to their terrestrial counterparts and source regions along the volcanic arcs. Additionally, we used the marine sedimentation rates in combination with tephra correlations to independently dated terrestrial deposits to build a chronotephrostratigraphy and obtained new ages for several eruptions already known on land. These data provide new insights into the overall lifetime and the number of major eruptions of the major volcanic centers in Guatemala and El Salvador. Volcanism in North Central America probably occurred in episodes since the Miocene with five pulses of enhanced activity during the Quaternary, the Pliocene (6–3 Ma), the Late Miocene (10–7 Ma), the Middle Miocene (17–11 Ma), and the Early Miocene (ca. >21 Ma).

Acknowledgments
The Integrated Ocean Discovery Program provided shipboard data and samples. We appreciate the help of IODP staff during sampling in College Station, TX. The German Research Foundation funded this project (grant KU-2685/2-1&2). We kindly thank K. Strehlow, I. Rohr, T. Wollenschläger, and K. Fockenberg for sample preparation and M. Thöner, J. Fietzke, D. Rau, F. Lin, Y. Chien, and C. Hung for lab assistance. We appreciate the comments from two anonymous reviewers, which helped to improve the manuscript. The authors declare no real or perceived financial conflicts of interests. All data are available in the supporting information.

References

Abers, G. A., Plank, T., & Hacker, B. R. (2003). The wet Nicaraguan slab. *Geophysical Research Letters*, *30*(2), 1098. https://doi.org/10.1029/2002GL015649

Ao, H., Roberts, A. P., Dekkers, M. J., Liu, X., Rohling, E. J., Shi, Z., et al. (2016). Late Miocene–Pliocene Asian monsoon intensification linked to Antarctic ice-sheet growth. *Earth and Planetary Science Letters*, *444*, 75–87. https://doi.org/10.1016/j.epsl.2016.03.028

Arana-Salinas, L., Siebe, C., & Macías, J. L. (2010). Dynamics of the ca. 4965 yr 14C BP "Ochre Pumice" Plinian eruption of Popocatépetl volcano, México. *Journal of Volcanology and Geothermal Research*, *192*(3–4), 212–231.

Arce, J., Cervantes, K., Macías, J., & Mora, J. (2005). The 12.1 ka Middle Toluca Pumice: A dacitic Plinian–subplinian eruption of Nevado de Toluca in central Mexico. *Journal of Volcanology and Geothermal Research*, *147*(1), 125–143.

Arce, J., Gardner, J., & Macías, J. (2013). Pre-eruptive conditions of dacitic magma erupted during the 21.7 ka Plinian event at Nevado de Toluca volcano, Central Mexico. *Journal of Volcanology and Geothermal Research*, *249*, 49–65.

Arce, J., Macías, J., Gardner, J., & Rangel, E. (2012). Reconstruction of the Sibinal Pumice, an andesitic Plinian eruption at Tacaná Volcanic Complex, Mexico–Guatemala. *Journal of Volcanology and Geothermal Research*, *217*, 39–55.

Arce, J. L., Macias, J. L., & Vázquez-Selem, L. (2003). The 10.5 ka Plinian eruption of Nevado de Toluca volcano, Mexico: Stratigraphy and hazard implications. *The Geological Society of America Bulletin*, *115*(2), 230–248.

Aubouin, J., Stephan, J.-F., Roump, J., & Renard, V. (1982). The middle america trench as an example of a subduction zone. *Tectonophysics*, *86*(1–3), 113,121,123–119,121,132. https://doi.org/10.1016/0040-1951(82)90063-4

Aubouin, J., & von Huene, R. (1985). Summary; leg 84, Middle America Trench transect off Guatemala and Costa Rica. *Initial reports of the Deep Sea Drilling Project covering Leg 84 of the cruises of the Drilling Vessel Glomar Challenger; Balboa, Panama, to Manzanillo, Mexico, January–February 1982, 84*, 939–957.

Barckhausen, U., Ranero, C. R., von Huene, R., Cande, S., & Roeser, H. (2001). Revised tectonic boundaries in the Cocos Plate off Costa Rica: Implications for the segmentation of the convergent margin and for plate tectonic models. *Journal of Geophysical Research*, *106*(19), 207–220.

Bloomfield, K., & Valastro, S. (1974). Late Pleistocene eruptive history of Nevado de Toluca volcano, central Mexico. *Geological Society of America Bulletin*, *85*(6), 901–906.

Bloomfield, K., & Valastro, S. Jr. (1977). *Late Quaternary tephrochronology of Nevado de Toluca volcano, central Mexico*. UK: Overseas Geology and Mineral Resources.

Boudal, C., & Robin, C. (1989). Volcán Popocatépetl: Recent eruptive history, and potential hazards and risks in future eruptions. In *Volcanic hazards*, (pp. 110–128). Berlin, Heidelberg: Springer.

Bowles, F. A., Jack, R. N., & Carmichael, I. S. E. (1973). Investigation of deep-sea volcanic ash layers from equatorial Pacific cores. *The Geological Society of America Bulletin*, *84*, 2371–2388.

Cadet, J.-P., Pouclet, A., Thisse, Y., Bardintzeff, J. M., & Azéma, J. (1982). In J. Aubouin, R. von Huene, et al. (Eds.), *Middle America Neogene explosive volcanism and ash layers: Evidence from the Middle America Trench transect, Deep Sea Drilling Project 67*, *Initial Reports DSDP*, (Vol. 67, pp. 475–491). Washington: U.S. Govt. Printing Office.

Cadet, J.-P., Thisse, Y., Pouclet, A., Bardintzeff, J.-M., & Stephan, J.-F. (1982). Tephra from Deep Sea Drilling Project leg 66; Middle America Trench transect (southern Mexico). *Leg 66 of the cruises of the drilling vessel Glomar Challenger; Mazatlan, Mexico to Manzanillo, Mexico; March–May, 1979, 66*, 687–698.

Cameron, B. I., Walker, J. A., Carr, M. J., Patino, L. C., Matias, O., & Feigenson, M. D. (2002). Flux versus decompression melting at stratovolcanoes in southeastern Guatemala. *Journal of Volcanology and Geothermal Research*, *119*, 21–50.

Carey, S., & Sigurdsson, H. (2000). Grain size of Miocene volcanic ash layers from sites 998, 999, and 1000: Implications for source areas and dispersal. In R. M. Leckie, H. Sigurdsson, G. D. Acton, & G. Draper (Eds.), *Proceedings ODP, Scientific Results*, (Vol. 165, pp. 101–110). College Station, TX.

Carey, S. N. (2000). Volcaniclastic sedimentation around island arcs. In H. E. A. Sigurdsson (Ed.), *Encyclopedia of volcanoes*, (pp. 627–642). New York: Academic Press.

Carr, M., Feigenson, M. D., Patino, L. C., & Walker, J. A. (2003). Volcanism and geochemistry in Central America: Progress and problems, inside the subduction factory. *AGU special publication, Geophysical Monograph*, *138*, 153–174.

Carr, M. J. (1984). Symetrical and segmented variation of physical and geochemical characteristics of the Central American Volcanic Front. *Journal of Volcanology and Geothermal Research*, *20*, 231–252.

Carr, M. J., Feigensohn, M. D., & Benett, E. A. (1990). Incompatible element and isotopic evidence for tectonic control of source mixing and melt extraction along the central American arc. *Contributions to Mineralogy and Petrology*, *105*, 369–380.

Carr, M. J., Patino, L. C., & Feigenson, M. D. (2007). Petrology and geochemistry of lavas. In J. Buntschuh, & G. E. Alvarado (Eds.), *Central America—Geology, resources and hazards*, (pp. 565–591). Rotterdam, Netherlands: Balkema.

Carrasco-Nunez, G., & Rose, W. I. (1995). Eruption of a major Holocene pyroclastic flow at Citlaltepetl volcano (Pico de Orizaba), Mexico, 8.5–9.0 ka. *Journal of Volcanology and Geothermal Research*, *69*, 197–215.

CEL (1992). Desarrollo de los Recursos Geotermicos del Area Centro-Occidental de El Salvador. Prefactibilidad Geotermica del Area de Coatepeque. Reconocimiento Geotermico: San Salvador, Commision Ejecutiva Hidroelectrica del Rio Lempa.

CEL (1995). Prestacion de Servicios de Consultoria para desarrollar Estudios Geocientificos Complementarios en el Campo Geotermico Berlin - Partida 4:Estudio Geovulcanica, y Recursos Geotermicos del Area Berlin-Chinameca. Prefactibilidad Geotermica del Area de Coatepeque. Reconocimiento Geotermico. Informe Definitivo. Internal report (contrado 2301). Retrieved from San Salvador.

Clift, P., & Vannucchi, P. (2004). Controls on tectonic accretion versus erosion in subduction zones: Implications for the origin and recycling of the continental crust. *Reviews of Geophysics*, *42*, RG2001. https://doi.org/10.1029/2003RG000127

Clift, P. D., Chan, L. H., Blusztajn, J., Layne, G. D., Kastner, M., & Kelly, R. K. (2005). Pulsed subduction accretion and tectonic erosion reconstructed since 2.5 Ma from the tephra record offshore Costa Rica. *Geochemistry, Geophysics, Geosystems*, *6*, Q09016. https://doi.org/10.1029/2005GC000963

Damon, P., & Montesinos, E. (1978). Late Cenozoic volcanism and metallogenesis over an active Benioff zone in Chiapas, Mexico. *Arizona Geological Society Digest*, *11*, 155–168.

Deligne, N. I., Coles, S. G., & Sparks, R. S. J. (2010). Recurrence rates of large explosive volcanic eruptions. *Journal of Geophysical Research*, *115*, B06203. https://doi.org/10.1029/2009JB006554

DeMets, C. (2001). A new estimate for present-day Cocos-Caribbean plate motion: Implications for slip along the Central American volcanic arc. *Geophysical Research Letters*, *28*, 4043–4046.

Donnelly, T. W., Horne, G. S., Finch, R. C., & López-Ramos, E. (1990). Northern Central America: The Maya and Chortis blocks. In J. E. Case, & G. Dengo (Eds.), *The geology of North America: The Caribbean Region*, (pp. 37–76). Boulder: The Geological Society of America.

Drexler, J. W., Rose, W. I. Jr., Sparks, R. S. J., & Ledbetter, M. T. (1980). The Los Chocoyos Ash, Guatemala: A major stratigraphic marker in Middle America and in the three ocean basins. *Quaternary Research*, *13*, 327–345.

Duffield, W. A., Tilling, R. I., & Canul, R. (1984). Geology of El Chichón Volcano, Chiapas, Mexico. *Journal of Volcanology and Geothermal Research*, *20*(1–2), 117–132.

Dull, R. A., Southon, J. R., & Sheets, P. D. (2001). Volcanism, Ecology and Culture: a Reassessment of the Volcán Ilopango TBJ Eruption in the Southern Maya Realm. *Latin American Antiquity*, *12*(1), 25–44.

Ehrenborg, J. (1996). A new stratigraphy for the Tertiary volcanic rocks of the Nicaraguan highland. *Geological Society of AmericanBulletin*, *108*, 830–842.

Espindola, J. M., Macias, J. L., Tilling, R. I., & Sheridan, M. F. (2000). Volcanic history of El Chichon volcano (Chiapas, Mexico) during the Holocene, and its impact on human activity. *Bulletin of Volcanology*, *62*, 90–104.

Feigenson, M. D., & Carr, M. J. (1986). Positively correlated Nd and Sr isotope ratios of lavas from the Central American volcanic front. *Geology*, *14*, 79–82.

Feigenson, M. D., Carr, M. J., Maharaj, S. V., Bolge, L. L., & Juliano, S. (2004). Lead isotope composition of Central American Volcanoes: Influence of the Galapagos Plume. *Geochemistry, Geophysics, Geosystems*, *5*, Q06001. https://doi.org/10.1029/2003GC000621

Ferrari, L. (2004). Slab detachment control on mafic volcanic pulse and mantle heterogeneity in central Mexico. *Geology*, *32*(1), 77–80.

Ferrari, L., López-Martínez, M., Aguirre-Díaz, G., & Carrasco-Núñez, G. (1999). Space-time patterns of Cenozoic arc volcanism in central Mexico: From the Sierra Madre Occidental to the Mexican Volcanic Belt. *Geology*, *27*(4), 303–306.

Ferrari, L., Orozco-Esquivel, T., Manea, V., & Manea, M. (2012). The dynamic history of the Trans-Mexican Volcanic Belt and the Mexico subduction zone. *Tectonophysics*, *522*, 122–149.

Ferriz, H., & Mahood, G. A. (1984). Eruption rates and compositional trends at Los Humeros volcanic center, Puebla, Mexico. *Journal of Geophysical Research*, *89*(B10), 8511–8524.

Fietzke, J., Liebetrau, V., Günther, D., Gürs, K., Hametner, K., Zumholz, K., et al. (2008). An alternative data acquisition and evaluation strategy for improved isotope ratio precision using LA-MC-ICP-MS applied to stable and radiogenic strontium isotopes in carbonates. *Journal of Analytical Atomic Spectrometry*, *23*(7), 955–961. https://doi.org/10.1039/b717706b

Freundt, A., Grevemeyer, I., Rabbel, W., Hansteen, T. H., Hensen, C., Wehrmann, H., et al. (2014). Volatile (H_2O, CO_2, Cl, S) budget of the Central American subduction zone. *International Journal of Earth Sciences*, *103*(7), 2101–2127. https://doi.org/10.1007/s00531-014-1001-1

Freundt, A., Kutterolf, S., Schmincke, H. U., Hansteen, T. H., Wehrmann, H., Perez, W., et al. (2006). Volcanic hazards in Nicaragua: Past, present, and future. In W. I. Rose, G. J. S. Bluth, M. J. Carr, J. Ewert, L. C. Patino, & J. W. Vallance (Eds.), *Volcanic hazards in Central America*. *The Geological Society of America, Special Publications*, *412*, 141–165. https://doi.org/10.1130/2006.2412(08)

Funk, J., Mann, P., McIntosh, K., & Stephens, J. (2009). Cenozoic tectonics of the Nicaraguan depression, Nicaragua, and Median Trough, El Salvador, based on seismic-reflection profiling and remote-sensing data. *Geological Society of America Bulletin*, *121*(11–12), 1491–1521.

García-Palomo, A., Macías, J., Tolson, G., Valdez, G., & Mora, J. (2002). Volcanic stratigraphy and geological evolution of the Apan region, east-central sector of the Trans-Mexican Volcanic Belt. *Geofisica Internacional Mexico*, *41*(2), 133–150.

Gardner, J. E., & Tait, S. (2000). The caldera-forming eruption of Volcan Ceboruco, Mexico. *Bulletin of Volcanology*, *62*(1), 20–33. https://doi.org/10.1007/s004450050288

Gazel, E., Carr, M., Hoernle, K., Feigenson, M. D., Szymanski, D., Hauff, F., & van den Bogard, P. (2009). Galapagos-OIB signature in southern Central America: Mantle refertilization by arc–hot spot interaction. *Geochemistry, Geophysics, Geosystems*, *10*, Q02S11. https://doi.org/10.1029/2008GC002246

Grützner, J., Rebesco, M., Cooper, A., Forsberg, C., Kryc, K., & Wefer, G. (2003). Evidence for orbitally controlled size variations of the East Antarctic ice sheet during the late Miocene. *Geology*, *31*(9), 777–780. https://doi.org/10.1130/G19574.1

Günther, D., Jackson, S. E., & Longerich, H. P. (1999). Laser ablation and arc/spark solid sample introduction into inductively coupled plasma mass spectrometers. *Spectrochimica Acta Part B: Atomic Spectroscopy*, *54*(3–4), 381–409. https://doi.org/10.1016/S0584-8547(99)00011-7

Hannah, R. S., Vogel, T. A., Patino, L. C., Alvarado, G. E., Perez, W., & Smith, D. R. (2002). Origin of silicic volcanic rocks in Central Costa Rica: A study of a chemically variable ash-flow sheet in the Tiribi tuff. *Bulletin of Volcanology*, *64*, 117–133.

Herbert, T. D., Lawrence, K. T., Tzanova, A., Peterson, L. C., Caballero-Gill, R., & Kelly, C. S. (2016). Late Miocene global cooling and the rise of modern ecosystems. *Nature Geoscience*, *9*(11), 843–847. https://doi.org/10.1038/ngeo2813

Heydolph, K., Hoernle, K., Hauff, F., Van den Bogaard, P., Portnyagin, M., Bindeman, I., & Garbe-Schönberg, D. (2012). Along and across arc geochemical variations in NW Central America: Evidence for involvement of lithospheric pyroxenite. *Geochimica et Cosmochimica Acta*, *84*, 459–491. https://doi.org/10.1016/j.gca.2012.01.035

Hoernle, K., Abt, D., Fischer, K., Nichols, H., Hauff, F., Abers, G., et al. (2008). Arc-parallel flow in the mantle wedge beneath Costa Rica and Nicaragua. *Nature*, *451*(7182), 1094–1097. https://doi.org/10.1038/nature06550

Hoernle, K., van den Bogaard, P., Werner, R., Lissinna, B., Alvarado, G. E., & Garbe-Schönberg, C.-D. (2002). Missing history (16-71 ma) of the Galapagos hotspot: Implications for the tectonic and biological evolution of the Americas. *Geology*, *30*(9), 795–798. https://doi.org/10.1130/0091-7613(2002)030<0795:MHMOTG>2.0.CO;2

Holbourn, A., Kuhnt, W., Schulz, M., & Erlenkeuser, H. (2005). Impacts of orbital forcing and atmospheric carbon dioxide on Miocene ice-sheet expansion. *Nature*, *438*(7067), 483–487. https://doi.org/10.1038/nature04123

Hoskuldsson, A., & Robin, C. (1993). Late Pleistocene to Holocene eruptive activity of Pico de Orizaba, eastern Mexico. *Bulletin of Volcanology*, *55*(8), 571–587. https://doi.org/10.1007/BF00301810

Hunt, J. B., & Hill, P. G. (2001). Tephrological implications of beam size—Sample-size effects in electron microprobe analysis of glass shards. *Journal of Quaternary Science*, *16*(2), 105–117. https://doi.org/10.1002/jqs.571

Jordan, B. R., Sigurdsson, H., Carey, S. N., Lundin, S., Rogers, R., Singer, B., & Barguero-Molina, M. (Eds) (2007). *Petrogenesis of Central American Tertiary ignimbrites and associated Caribbean Sea tephra*, *GSA Special papers*. Austin, TX: Geological Society of Amercia.

Jordan, B. R., Sigudsson, H., Carey, S. N., Rogers, R., & Ehrenborg, J. (2006). Geochemical correlation of Caribbean Sea tephra layers with ignimbrites in Central America. In C. Siebe, J. L. Macías, & G. J. Aguirre-Díaz (Eds.), *Neogene-Quaternary continental margin volcanism: A perspective from México*, (Vol. 402, pp. 175–208). Boulder, CO.

Jordan, B. R., Sigurdsson, H., Carey, S. N., Rogers, R., & Ehrenborg, J. (2007). Geochemical variation along and across the central American Miocene paleoarc in Honduras and Nicaragua. *Geochimica et Cosmochimica Acta*, *71*(14), 3581–3591. https://doi.org/10.1016/j.gca.2007.05.013

Keller, J., Ryan, W. B. F., Ninkovich, D., & Altherr, R. (1978). Explosive volcanic activity in the Mediterranian over the past 200.000 years as recorded in deep-sea sediments. *The Geological Society of America Bulletin*, *89*(4), 591–604. https://doi.org/10.1130/0016-7606(1978)89<591:EVAITM>2.0.CO;2

Kennett, J. P., McBirney, A. R., & Thunell, R. C. (1977). Episodes of Cenozoic volcanism in the circum-Pacific region. *Journal of Volcanology and Geothemal Research*, *2*(2), 145–163. https://doi.org/10.1016/0377-0273(77)90007-5

Kennett, J. P., & Thunell, R. C. (1975). Global increase in quaternary explosive volcanism. *Science*, *187*(4176), 497–502. https://doi.org/10.1126/science.187.4176.497

Koch, A. J., & McLean, H. (1975). Pleistocene tephra and ash-flow deposits in the volcanic highlands of Guatemala. *The Geological Society of America Bulletin*, *86*(4), 529–541. https://doi.org/10.1130/0016-7606(1975)86<529:PTAADI>2.0.CO;2

Kohn, M. J., & Fremd, T. J. (2008). Miocene tectonics and climate forcing of biodiversity, western United States. *Geology*, *36*(10), 783–786. https://doi.org/10.1130/G24928A.1

Kutterolf, S., Freundt, A., & Burkert, C. (2011). Eruptive history and magmatic evolution of the 1.9 kyr Plinian dacitic Chiltepe tephra from Apoyeque volcano in west-Central Nicaragua. *Bulletin of Volcanology*, *73*(7), 811–831. https://doi.org/10.1007/s00445-011-0457-0

Kutterolf, S., Freundt, A., & Peréz, W. (2008). The Pacific offshore record of Plinian arc volcanism in Central America, part 2: Tephra volumes and erupted masses. *Geochemistry, Geophysics, Geosystems*, *9*, Q02S02. https://doi.org/10.1029/2007GC001791

Kutterolf, S., Freundt, A., Peréz, W., Mörz, T., Schacht, U., Wehrmann, H., & Schmincke, H.-U. (2008). The Pacific offshore record of Plinian arc volcanism in Central America, part 1: Along-arc correlations. *Geochemistry, Geophysics, Geosystems*, *9*, Q02S01. https://doi.org/10.1029/2007GC001631

Kutterolf, S., Freundt, A., Schacht, U., Bürk, D., Harders, R., Mörz, T., & Peréz, W. (2008). The Pacific offshore record of Plinian arc volcanism in Central America, part 3: Application to forearc geology. *Geochemistry, Geophysics, Geosystems*, *9*, Q02S03. https://doi.org/10.1029/2007GC001826

Kutterolf, S., Jegen, M., Mitrovica, J. X., Kwasnitschka, T., Freundt, A., & Huybers, P. (2013). A detection of Milankovitch frequencies in global volcanic activity. *Geology*, *41*(2), 227–230. https://doi.org/10.1130/G33419.1

Kutterolf, S., Liebetrau, V., Moerz, T., Freundt, A., Hammerich, T., & Garbe-Schönberg, D. (2008). Lifetime and cyclicity of fluid venting at forearc mound structures determined by tephrostratigraphy and radiometric dating of authigenic carbonates. *Geology*, *36*(9), 707–710. https://doi.org/10.1130/G24806A.1

Kutterolf, S., Schacht, U., Wehrmann, H., Freundt, A., & Mörz, T. (2007). Onshore to offshore tephrostratigraphy and marine ash layer diagenesis in Central America. In J. Buntschuh, & G. E. Alvarado (Eds.), *Central America—Geology, resources and hazards*, (Vol. 2, pp. 395–423). Lisse, Niederlande, Tokio, Japan: Balkema. https://doi.org/10.1201/9780203947043.ch14

Kutterolf, S., Schindlbeck, J. C., Anselmetti, F. S., Ariztegui, D., Brenner, M., Curtis, J., et al. (2016). A 400-ka tephrochronological framework for Central America from Lake Petén Itzá (Guatemala) sediments. *Quaternary Science Reviews*, *150*, 200–220. https://doi.org/10.1016/j.quascirev.2016.08.023

Kutterolf, S., Schindlbeck, J. C., Robertson, A. H. F., Avery, A., Baxter, A. T., Petronotis, K., & Wang, K. L. (2018). Tephrostratigraphy and provenance from IODP expedition 352, Izu-Bonin Arc: Tracing tephra sources and volumes from the Oligocene to Recent. *Geochemistry, Geophysics, Geosystems*, *19*, 150–174. https://doi.org/10.1002/2017GC007100

Kutterolf, S., Schindlbeck, J. C., Scudder, R. P., Murray, R. W., Pickering, K. T., Freundt, A., et al. (2014). Large volume submarine ignimbrites in the Shikoku Basin: An example for explosive volcanism in the Western Pacific during the Late Miocene. *Geochemistry, Geophysics, Geosystems*, *15*, 1837–1851. https://doi.org/10.1002/2014gc005263

Kwasnitschka, T. (2009). Volcanic and tectonic development of the Ilopango Caldera, El Salvador: Stratigraphic correlation and visulization of emplacement. Diploma tesis, University of Kiel, pp. 157.

Le Maitre, R. W., Streckeisen, A., Zanettin, B., Le Bas, M. J., Bonin, B., & Bateman, P. (2002). *Igneous rocks: A classification and glossary of terms*. Cambridge, UK: Cambridge University Press. https://doi.org/10.1017/CBO9780511535581

Ledbetter, M. T. (1985). Tephrochronology of marine tephra adjacent to Central America. *The Geological Society of America Bulletin*, *96*(1), 77–82. https://doi.org/10.1130/0016-7606(1985)96<77:TOMTAT>2.0.CO;2

Lenhardt, N., Böhnel, H., Wemmer, K., Torres-Alvarado, I. S., Hornung, J., & Hinderer, M. (2010). Petrology, magnetostratigraphy and geochronology of the Miocene volcaniclastic Tepoztlán formation: Implications for the initiation of the Transmexican Volcanic Belt (Central Mexico). *Bulletin of Volcanology*, *72*(7), 817–832. https://doi.org/10.1007/s00445-010-0361-z

Lenhardt, N., Hornung, J., Hinderer, M., Böhnel, H., Torres-Alvarado, I. S., & Trauth, N. (2011). Build-up and depositional dynamics of an arc front volcaniclastic complex: The Miocene Tepoztlán formation (Transmexican Volcanic Belt, Central Mexico). *Sedimentology*, *58*(3), 785–823. https://doi.org/10.1111/j.1365-3091.2010.01203.x

Lexa, J., Sebesta, J., Chávez, J. A., Hernández, W., & Pecskay, Z. (2011). Geology and volcanic evolution in the southern part of the San Salvador Metropolitan Area. *Journal of Geosciences*, *56*(1), 106–140.

Lowe, D. J. (2011). Tephrochronology and its application: A review. *Quaternary Geochronology*, *6*, 107–153.

Luhr, J. F., Kimberly, P., Siebert, L., Aranda-Gómez, J. J., Housh, T. B., & Mattietti, G. K. (2006). México's Quaternary volcanic rocks: Insights from the MEXPET petrological and geochemical database. In C. Siebe, J. L. Macias, & G. J. Aguirre-Diaz (Eds.), *Neogene-Quaternary continental margin volcanism: A perspective from México* (Vol. 402, pp. 1–44). Boulder: The Geological Society of America.

Macías, J., Arce, J., Mora, J., Espíndola, J., Saucedo, R., & Manetti, P. (2003). A 550-year-old Plinian eruption at El Chichón volcano, Chiapas, Mexico: Explosive volcanism linked to reheating of the magma reservoir. *Journal of Geophysical Research*, *108*(B12), 2569. https://doi.org/10.1029/2003JB002551

Mahony, S. H., Sparks, R. S. J., Wallace, L. M., Engwell, S. L., Scourse, E. M., Barnard, N. H., et al. (2016). Increased rates of large-magnitude explosive eruptions in Japan in the late Neogene and Quaternary. *Geochemistry, Geophysics, Geosystems*, *17*, 2467–2479. https://doi.org/10.1002/2016GC006362

Mahood, G. A. (1981). Chemical evolution of a Pleistocene rhyolitic center: Sierra La primavera, Jalisco, Mexico. *Contributions to Mineralogy and Petrology*, *77*(2), 129–149. https://doi.org/10.1007/BF00636517

Mahood, G. A., & Halliday, A. N. (1988). Generation of high-silica rhyolite: A Nd, Sr, and O isotopic study of sierra La primavera, Mexican Neovolcanic Belt. *Contributions to Mineralogy and Petrology*, *100*(2), 183–191. https://doi.org/10.1007/BF00373584

Mann, C. P., Stix, J., Vallance, J. W., & Richer, M. (2004). Subaqueous intracaldera volcanism, Ilopango Caldera, El Salvador, Cental America. In W. I. Rose, J. J. Bommer, D. L. López, M. J. Carr, & J. J. Major (Eds.), *Natural hazards in El Salvador*, (Vol. 375, pp. 159–174). Boulder, Colorado: The Geological Society of America Special Publications. https://doi.org/10.1130/0-8137-2375-2.159

Mann, P., Rogers, R. D., & Gahagan, L. (2007). Overview of plate tectonic history and its unresolved tectonic problems. In J. Buntschuh, & G. E. Alvarado (Eds.), *Central America—Geology, resources and hazards*, (Vol. 2, pp. 201–238). Lisse, Niederlande, Tokio, Japan: Balkema.

Márquez, A., Oyarzun, R., Doblas, M., & Verma, S. P. (1999). Alkalic (ocean-island basalt type) and calc-alkalic volcanism in the Mexican volcanic belt: A case for plume-related magmatism and propagating rifting at an active margin? *Geology*, *27*(1), 51–54. https://doi.org/10.1130/0091-7613(1999)027<0051:AOIBTA>2.3.CO;2

Mason, B. G., Pyle, D. M., & Oppenheimer, C. (2004). The size and frequency of the largest explosive eruptions on earth. *Bulletin of Volcanology*, *66*(8), 735–748. https://doi.org/10.1007/s00445-004-0355-9

Mayer, L., Pisias, N., Kanecek, T., & Al, E. (1992). *Proceedings of ODP, Initial Reports*, (Vol. 138). College Station, TX: Ocean Drilling Program. https://doi.org/10.2973/odp.proc.ir.138.1992

McGuire, W. J., Howarth, R. J., Firth, C. R., Solow, A. R., Pullen, A. D., Saunders, S. J., et al. (1997). Correlation between rate of sea-level change and frequency of explosive volcanism in the Mediterranean. *Nature*, *389*(6650), 473–476. https://doi.org/10.1038/38998

Moore, G., Marone, C., Carmichael, I. S., & Renne, P. (1994). Basaltic volcanism and extension near the intersection of the Sierra Madre volcanic province and the Mexican Volcanic Belt. *Geological Society of America Bulletin*, *106*(3), 383–394. https://doi.org/10.1130/0016-7606(1994)106<0383:BVAENT>2.3.CO;2

Mora, J., Jaimes-Viera, M., Garduño-Monroy, V., Layer, P., Pompa-Mera, V., & Godinez, M. (2007). Geology and geochemistry characteristics of the Chiapanecan volcanic arc (central area), Chiapas Mexico. *Journal of Volcanology and Geothermal Research*, *162*(1-2), 43–72. https://doi.org/10.1016/j.jvolgeores.2006.12.009

Morán-Zenteno, D. J., Tolson, G., Martınez-Serrano, R., Martiny, B., Schaaf, P., Silva-Romo, G., et al. (1999). Tertiary arc-magmatism of the Sierra Madre del Sur, Mexico, and its transition to the volcanic activity of the trans-Mexican Volcanic Belt. *Journal of South American Earth Sciences*, *12*(6), 513–535. https://doi.org/10.1016/S0895-9811(99)00036-X

Nelson, S. A., & Gonzales-Caver, E. (1992). Geology and K-Ar dating of the Tuxtla volcanic field, Veracruz, Mexico. *Bulletin of Volcanology*, *55*(1-2), 85–96. https://doi.org/10.1007/BF00301122

Neugebauer, I., Wulf, S., Schwab, M. J., Serb, J., Plessen, B., Appelt, O., & Brauer, A. (2017). Implications of S1 tephra findings in Dead Sea and Tayma palaeolake sediments for marine reservoir age estimation and palaeoclimate synchronisation. *Quaternary Science Reviews*, *170*, 269–275. https://doi.org/10.1016/j.quascirev.2017.06.020

Newhall, C. G. (1987). Geology of the Lake Atitlàn region, Western Guatemala. *Journal of Volcanology and Geothermal Research*, *33*(1-3), 23–55. https://doi.org/10.1016/0377-0273(87)90053-9

Newton, A. J., & Metcalfe, S. E. (1999). Tephrochronology of the Toluca Basin, Central Mexico. *Quaternary Science Reviews*, *18*(8-9), 1039–1059. https://doi.org/10.1016/S0277-3791(98)00043-2

Norman, M., Pearson, N., Sharma, A., & Griffin, W. (1996). Quantitative analysis of trace elements in geological materials by laser ablation ICPMS: Instrumental operating conditions and calibration values of NIST glasses. *Geostandards Newsletter*, *20*(2), 247–261. https://doi.org/10.1111/j.1751-908X.1996.tb00186.x

Nyström, J. O., Levy, B., Troeng, B., Ehrenborg, J., & Carranza, G. (1988). Geochemistry of volcanic rocks in a traverse through Nicaragua. *Revista Geologica de America Central*, *8*, 77–109.

Ortega-Guerrero, B., & Newton, A. J. (1998). Geochemical characterization of Late Pleistocene and Holocene tephra layers from the basin of Mexico, Central Mexico. *Quaternary Research*, *50*(01), 90–106. https://doi.org/10.1006/qres.1998.1975

Partida, E. G., Rodríguez, V. T., & Birkle, P. (1997). Plio-Pleistocene volcanic history of the Ahuachapan geothermal system, El Salvador: The Concepción de Ataco caldera. *Geothermics*, *26*(5–6), 555–575. https://doi.org/10.1016/S0375-6505(97)00018-7

Patino, L. C., Carr, M., & Feigenson, M. D. (1997). Cross-arc geochemical variations in volcanic fields in Honduras CA: Progressive changes in source with distance from the volcanic front. *Contributions to Mineralalogy and Petrology*, *129*(4), 341–351. https://doi.org/10.1007/s004100050341

Patino, L. C., Carr, M., & Feigenson, M. D. (2000). Local and regional variations in central American arc lavas controlled by variations in subducted sediment input. *Contributions to Mineralalogy and Petrology*, *138*, 256–283.

Petersen, P. S., & Rose, W. I. (1985). Explosive eruptions of the Ayarza calderas, southeastern Guatemala. *Journal of Volcanology and Geothermal Research*, *25*, 289–307.

Plank, T., Balzer, V., & Carr, M. (2002). Nicaraguan volcanoes record paleoceanographic changes accompanying closure of the Panama gateway. *Geology*, *30*(12), 1087–1090. https://doi.org/10.1130/0091-7613(2002)030<1087:NVRPCA>2.0.CO;2

Plank, T., & Langmuir, C. H. (1988). An evaluation of the global variations in the major element chemistry of arc basalts. *Earth and Planetary Science Letters*, *90*(4), 349–370. https://doi.org/10.1016/0012-821X(88)90135-5

Ponomareva, V., Polyak, L., Portnyagin, M., Abbott, P. M., Zelenin, E., Vakhrameeva, P., & Garbe-Schönberg, D. (2017). Holocene tephra from the Chukchi-Alaskan margin, Arctic Ocean: Implications for sediment chronostratigraphy and volcanic history. *Quaternary Geochronology*, *45*, 85–97. https://doi.org/10.1016/j.quageo.2017.11.001

Ponomareva, V., Portnyagin, M., & Davies, S. M. (2015). Tephra without borders: Far-reaching clues into past explosive eruptions. *Frontiers in Earth Science*, *3*, 83.

Ponomareva, V., Portnyagin, M., Derkachev, A., Pendea, I. F., Bourgeois, J., Reimer, P. J., et al. (2013). Early Holocene M~ 6 explosive eruption from Plosky volcanic massif (Kamchatka) and its tephra as a link between terrestrial and marine paleoenvironmental records. *International Journal of Earth Sciences*, *102*(6), 1673–1699. https://doi.org/10.1007/s00531-013-0898-0

Pyle, D. M. (1995). Mass and energy budgets of explosive volcanic eruptions. *Geophysical Research Letters*, *22*(5), 563–566. https://doi.org/10.1029/95gl00052

Rabek, K., Ledbetter, M. T., & Williams, D. F. (1985). Tephrochronology of the Western Gulf of Mexico. *Quaternary Research*, *23*(03), 403–416. https://doi.org/10.1016/0033-5894(85)90044-4

Rampino, M. R., Self, S., & Fairbridge, R. W. (1979). Can rapid climatic change cause volcanic eruptions? *Science*, *206*(4420), 826–829. https://doi.org/10.1126/science.206.4420.826

Reynolds, J. H. (1980). Late tertiary volcanic stratigraphy of northern Central America. *Bulletin of Volcanology*, *43*(3), 601–607. https://doi.org/10.1007/BF02597696

Reynolds, J. H. (1987). Timing and sources of Neogene and quaternary volcanism in south-Central Guatemala. *Journal of Volcanology and Geothermal Research*, *33*(1-3), 9–22. https://doi.org/10.1016/0377-0273(87)90052-7

Robin, C., & Cantagrel, J. (1982). Le Pico de Orizaba (Mexique): Structure et evolution d'un grand volcán andesitique complexe. *Bulletin Volcanologique*, *45*(4), 299–315. https://doi.org/10.1007/BF02597254

Robin, C., Cantagrel, J., & Vincent, P. (1983). Les nuées ardentes de type Saint-Vincent, épisodes remarquables de l'évolution récente du Pico de Orizaba (Mexique). *Bulletin de la Société Géologique de France*, *7*(5), 727–736.

Robin, C., Mossand, P., Camus, G., Cantagrel, J.-M., Gourgaud, A., & Vincent, P. M. (1987). Eruptive history of the Colima volcanic complex (Mexico). *Journal of Volcanology and Geothermal Research*, *31*(1-2), 99–113. https://doi.org/10.1016/0377-0273(87)90008-4

Rogers, R. D., Kárason, H., & van der Hilst, R. D. (2002). Epeirogenic uplift above a detached slab in northern Central America. *Geology*, *30*(11), 1031–1034.

Rohr, I. (2014). *Stratigraphy and depositional processes of the 72 ka old Arce tephra, Coatepeque Calder (El Salvador) Part 2: Ignimbrites and fallouts of the upper sequence*. (Master Thesis, pp. 71) Christian-Albrechts-Universität zu Kiel, Kiel.

Rose, W. I., Conway, F. M., Pullinger, C. R., Deino, A., & McIntosh, K. (1999). An improved age framework for late Quaternary silicic eruptions in northern Central America. *Bulletin of Volcanology*, *61*(1-2), 106–120. https://doi.org/10.1007/s004450050266

Rose, W. I., Newhall, C. G., Bornhorst, T. J., & Self, S. (1987). Quaternary silicic pyroclastic deposits of Atitlàn caldera, Guatemala. *Journal of Volcanology and Geothermal Research*, *33*(1-3), 57–80. https://doi.org/10.1016/0377-0273(87)90054-0

Rossotti, A., Carrasco-Núñez, G., Rosi, M., & Di Muro, A. (2006). Eruptive dynamics of the "Citlaltépetl pumice" at Citlaltépetl volcano, eastern Mexico. *Journal of Volcanology and Geothermal Research*, *158*(3–4), 401–429. https://doi.org/10.1016/j.jvolgeores.2006.07.008

Ryan, W. B. F., Carbotte, S. M., Coplan, J. O., O'Hara, S., Melkonian, A., Arko, R., et al. (2009). Global multi-resolution topography synthesis. *Geochemistry, Geophysics, Geosystems*, *10*, Q03014. https://doi.org/10.1029/2008gc002332

Schindlbeck, J. C., Kutterolf, S., Freundt, A., Alvarado, G. E., Wang, K. L., Straub, S. M., et al. (2016). Late Cenozoic tephrostratigraphy offshore the southern central American volcanic arc: 1. Tephra ages and provenance. *Geochemistry, Geophysics, Geosystems*, *17*, 4585–4604. https://doi.org/10.1002/2016GC006504

Schindlbeck, J. C., Kutterolf, S., Freundt, A., Andrews, G., Wang, K.-L., Völker, D., et al. (2016). Alkalic marine tephra layers at ODP site 1241-major explosive eruptions from an oceanic volcano in a pre-shield stage? *Journal of Volcanology and Geothermal Research*, *328*, 96–104. https://doi.org/10.1016/j.jvolgeores.2016.10.009

Schindlbeck, J. C., Kutterolf, S., Freundt, A., Straub, S., Vannucchi, P., & Alvarado, G. (2016). Late Cenozoic tephrostratigraphy offshore the southern central American volcanic arc: 2. Implications for magma production rates and subduction erosion. *Geochemistry, Geophysics, Geosystems*, *17*, 4641–4668. https://doi.org/10.1002/2016GC006503

Schindlbeck, J. C., Kutterolf, S., Freundt, A., Straub, S. M., Wang, K.-L., Jegen, M., et al. (2015). The Miocene Galápagos ash layer record of Integrated Ocean drilling program legs 334 and 344: Ocean-island explosive volcanism during plume-ridge interaction. *Geology*, *43*(7), 599–602. https://doi.org/10.1130/g36645.1

Schindlbeck, J. C., Kutterolf, S., Straub, S. M., Andrews, G. D. M., Wang, K.-L., & Mleneck-Vautravers, M. J. (2018). One million years tephra record at IODP sites U1436 and U1437: Insights into explosive volcanism from the Japan and Izu arcs. *Island Arc*, *27*(3), e12244. https://doi.org/10.1111/iar.12244

Sheth, H. C., Torres-Alvarado, I. S., & Verma, S. P. (2000). Beyond subduction and plumes: A unified tectonic-petrogenetic model for the Mexican volcanic belt. *International Geology Review*, *42*(12), 1116–1132. https://doi.org/10.1080/00206810009465129

Siebe, C., Abrams, M., Macías, J. L., & Obenholzner, J. (1996). Repeated volcanic disasters in Prehispanic time at Popocatepetl, Central Mexico: Past key to the future? *Geology*, *24*(5), 399–402. https://doi.org/10.1130/0091-7613(1996)024<0399:RVDIPT>2.3.CO;2

Siebe, C., Macias, J. L., Abrams, M., Rodriguez, S., Castro, R., & Delgado, H. (1995). *Quaternary explosive volcanism and pyroclastic deposits in east central Mexico: implications for future hazards*. Paper presented at the Guidebook of geological excursions: in conjunction with the Annual Meeting of the Geological Society of America, New Orleans, Louisiana, November 6–9, 1995.

Siebert, L., Simkin, T., & Kimberly, P. (2010). *Volcanoes of the world*. Berkeley: University of California Press.

Sieron, K., Capra, L., & Rodríguez-Elizararrás, S. (2014). Hazard assessment at San Martín volcano based on geological record, numerical modeling, and spatial analysis. *Natural Hazards*, *70*(1), 275–297. https://doi.org/10.1007/s11069-013-0807-7

Sigurdsson, H. (1990). Evidence of volcanic loading of the atmosphere and climate response. *Global and Planetary Change*, *3*(3), 277–289.

Sigurdsson, H., Kelley, R. M., Carey, S., Bralower, T., & King, J. (2000). History of circum-Caribbean explosive volcanism: $^{40}Ar/^{39}Ar$ dating of tephra layers. *Proceedings of ODP Scientific Results*, *165*.

Stoppa, L. (2015). *Tephrachronostratigraphy of the Malpaisillo Caldera (Central-western Nicaragua)*. (Master Thesis, pp. 73), Université de Fribourg, Fribourg.

Stoppa, L., Kutterolf, S., Rausch, J., Grobety, B., Pettke, T., Wang, K.-L., & Hemming, S. (2018). The Malpaisillo formation: A sequence of explosive eruptions in the mid to late Pleistocene (Nicaragua, Central America). *Journal of Volcanology and Geothermal Research*, *359*, 47–67. https://doi.org/10.1016/j.jvolgeores.2018.06.015

Syracuse, E. M., & Abers, G. A. (2006). Global compilation of variations in slab depth beneath arc volcanoes and implications. *Geochemistry, Geophysics, Geosystems*, *7*, Q05017. https://doi.org/10.1029/2005gc001045

van Achterberg, E., Ryan, C. G., Jackson, S. E., & Griffin, W. (2001). LA-ICP-MS in the earth sciences - appendix 3, data reduction software for LA-ICP-MS. In P. J. Sylvester (Ed.), *Short course volume 29: St.John's, Mineralogical Association of Canada*, (pp. 239–243). Ottawa, Ontario.

Verma, S. P. (2002). Absence of Cocos plate subduction-related basic volcanism in southern Mexico: A unique case on earth? *Geology*, *30*(12), 1095–1098. https://doi.org/10.1130/0091-7613(2002)030<1095:AOCPSR>2.0.CO;2

Verma, S. P. (2006). Extension-related origin of magmas from a garnet-bearing source in the Los Tuxtlas volcanic field, Mexico. *International Journal of Earth Sciences*, *95*(5), 871–901. https://doi.org/10.1007/s00531-006-0072-z

Verma, S. P., & Carrasco-Núñez, G. (2003). Reappraisal of the geology and geochemistry of Volcán Zamorano, Central Mexico: Implications for discriminating the Sierra Madre occidental and Mexican Volcanic Belt provinces. *International Geology Review*, *45*(8), 724–752. https://doi.org/10.2747/0020-6814.45.8.724

von Huene, R., Aubouin, J., & Al, E. (1985). Initial reports DSDP, 84. Retrieved from Washington, U.S. Government Printing Office.

Von Huene, R., & Scholl, D. W. (1991). Observations at convergent margins concerning sediment subduction, subduction erosion, and the growth of continental crust. *Reviews of Geophysics*, *29*(3), 279–316.

Walker, J., Mickelson, E., Thomas, R. B., Patino, L. C., Cameron, B., Carr, M. J., et al. (2007). U-series disequilibria in Guatemalan lavas, crustal contamination, and implications for magma genesis along the central American subduction zone. *Journal of Geophysical Research*, *112*, B06205. https://doi.org/10.1029/2006JB004589

Watkins, J. S., Moore, J. C., & Al, E. (1981). Initial reports DSDP, 66. Retrieved from Washington, U.S. Government Printing Office.

Weyl, R. (1980). Geology of Central America. In F. E. A. Bender (Ed.), *Beitra€ge zur regionalen Geologie der Erde* (2nd ed., Vol. 15, 371 pp.). Berlin: Gebr. Borntraeger.

Wise, S. A., & Watters, R. L. (2012). Certificate of Analysis, Standard Reference Material 610. National Institute of Standards and Technology.

Wulf, S., Kraml, M., Brauer, A., Keller, J., & Negendank, J. F. W. (2004). Tephrochronology of the 100 ka lacustrine sediment record of Lago Grande di Monticchio (southern Italy). *Quaternary International*, *122*(1), 7–30. https://doi.org/10.1016/j.quaint.2004.01.028

Zachos, J., Pagani, M., Sloan, L., Thomas, E., & Billups, K. (2001). Trends, rhythms, and aberrations in global climate 65 Ma to present. *Science*, *292*(5517), 686–693.